A multi-model analysis of the decadal prediction skill for the North Atlantic ocean heat content

Teresa Carmo-Costa[1], Roberto Bilbao[2], Jon Robson[3], Ana Teles-Machado[1,4], and Pablo Ortega[2]

[1]Faculdade de Ciências da Universidade de Lisboa - Instituto Dom Luiz, Lisbon, Portugal
[2]Barcelona Supercomputing Center, Barcelona, Spain
[3]National Centre for Atmospheric Science, University of Reading, Reading, UK
[4]Instituto Português do Mar e da Atmosfera, Lisbon, Portugal

Correspondence: Teresa Carmo-Costa (tmcosta@fc.ul.pt) and Pablo Ortega (pablo.ortega@bsc.es)

Abstract. Decadal predictions can skillfully forecast upper ocean temperatures in many regions worldwide. The North Atlantic, in particular, shows high predictive skill for the Ocean Heat Content (OHC). This multi-model study analyzes eight CMIP6 climate models with comparable decadal prediction (DCPP) and historical (HIST) ensembles to document differences in North Atlantic upper OHC skill and investigates the underlying causes. The decadal predictions consistently identify two main regions with high predictive capacity and added value of initialization: the Labrador Sea and the Eastern North Atlantic. A region east of the Grand Banks is also found to exhibit negative skill scores, with its extent and location varying widely across models, possibly due in part to observational uncertainties affecting both forecast verification and local initialization.

Special attention is given to the Labrador Sea and its surroundings, a region characterized by high inter-model spread in OHC prediction skill in both DCPP and HIST experiments. These differences hinder the identification of the relative contributions of external forcings and internal variability to local OHC predictability. To address this, we explore the relationship between the local OHC skill in the HIST ensemble and various mean-state properties in the Labrador Sea, revealing a strong link between the skill in those experiments and both the mean local surface fluxes and density stratification.

Benchmarking these mean-state properties against observations and reanalyses suggests that the multi-model mean likely offers the most realistic estimate of the forced signal, accounting for approximately 16% of the total OHC variance in the Labrador Sea. These findings underscore the critical role of stratification and atmospheric forcing biases in shaping predictive skill and highlight the potential of multi-model ensembles to advance our understanding of decadal predictability.

1 Introduction

The global oceans have absorbed approximately 93% of the excess energy in the climate system over the recent decades (e.g. IPCC, 2021, and citations therein). This energy accumulation is commonly quantified by the ocean heat content, a vertically integrated variable that captures changes in heat storage within the ocean. Among the regions with significant warming, the

North Atlantic (NA) ocean stands out for its pronounced increase in OHC within the upper 2000m since the 1960s (e.g. Levitus et al., 2000, 2012; Palmer et al., 2007; Durack et al., 2018; Zanna et al., 2019; Johnson and Lyman, 2020). While the slow nature of past OHC changes provides a high degree of predictability, considerable uncertainty remains across observational products regarding their geographical distribution (e.g. Häkkinen et al., 2015; Palmer et al., 2017), which can limit their local predictive skill. This study aims to improve our understanding of the factors controlling OHC predictability in the NA.

The warming trends that the upper layers of the NA ocean has experienced over the last 70 years can be largely explained by changes in anthropogenic forcings (e.g. Gleckler et al., 2012; Bilbao et al., 2019). However, the distribution of OHC trends is not geographically uniform and some regions have exhibited considerable multi-decadal variability (e.g. Carmo-Costa et al., 2021). While most of the NA ocean has warmed, the center of the Subpolar North Atlantic (SPNA) has been subject to a long-term cooling trend (e.g. Johnson and Lyman, 2020) typically referred to as the NA warming hole (Drijfhout et al., 2012; Rahmstorf et al., 2015; Keil et al., 2020). This phenomenon has been primarily characterized using sea surface temperature (SST) observations. The main mechanism proposed to explain the cooling involves a reduction in northward heat advection, in turn responding to either a shift in the North Atlantic gyre circulation (Piecuch et al., 2017) or a weakening of the Atlantic Meridional Overturning Circulation (AMOC) (Drijfhout et al., 2012; Rahmstorf et al., 2015; Robson et al., 2016; Keil et al., 2020), which might have emerged in response to the increasing greenhouse gas concentrations (Caesar et al., 2021).

Internal variability in the North Atlantic region could also explain some of the regional changes in the OHC. The North Atlantic Oscillation (NAO) is an important driver of AMOC variability through its influence on Labrador Sea deep water formation. Positive NAO phases enhance winter surface cooling and can thus help overcome the local vertical density stratification, promoting the occurrence of deep ocean mixing events. In addition, interannual NAO variations are also known to force local OHC anomalies across the North Atlantic subpolar gyre mediated via changes in the surface buoyancy fluxes and wind stress (Oldenburg et al., 2021). An illustrative example was the record-breaking cold anomaly that the central SPNA experienced in spring 2015 (commonly referred to as the Cold Blob (Yeager et al., 2016; Josey et al., 2018)), emerging in response to exceptionally rare (both in terms of magnitude and persistence) positive NAO conditions (Yeager, 2020; Maroon et al., 2021) which enhanced local heat loss. This extremely cold central SPNA state has been linked to the occurrence of a major heatwave in Central Europe in the summer of 2015 (Mecking et al., 2019). Likewise, the broader North Atlantic region exhibits significant multidecadal variability, which is particularly prominent in sea surface temperatures, but also affects the OHC (Moat et al., 2024). These variations have been linked to numerous climate impacts, including the intensity and frequency of Atlantic hurricane activity and Sahel rainfall (Balaguru et al., 2018; Buckley and Marshall, 2016; Zhang and Delworth, 2006), as well as hydroclimate and temperature conditions in North America and Europe (Enfield et al., 2001; Sutton and Hodson, 2005; Kwon et al., 2020; Josey et al., 2018).

Understanding the causes of the regional OHC changes in the North Atlantic, by disentangling the contributions from internal and externally forced variability and the underlying uncertainties is, therefore, crucial to better anticipate how the climate will evolve in the coming years. There are two major types of simulations within the Climate Model Intercomparison Project phase 6 initiative (CMIP6 Eyring et al., 2016) that can be jointly used to understand the contributions of external forcings and internal variability processes to the recent climate evolution and to understand the sources of predictability of the North Atlantic's

ocean-atmosphere system (Meehl et al., 2014): historical simulations and decadal predictions. While historical experiments are designed to investigate how the Earth system responded to recent changes in external radiative forcings and evaluate the mean model performance against observations (Eyring et al., 2016), retrospective decadal predictions performed under the Decadal Climate Prediction Project (DCPP; Boer et al., 2016) serve to assess our ability to skilfully predict climate variations from one year up to a decade ahead. Both historical and DCPP experiments use the same prescribed external radiative forcings, but differ in one major aspect: the decadal predictions are initialized to align their starting conditions with a past observed state, which allows them to benefit, in theory, from the predictability arising from internal variability sources. In contrast, historical ensembles are designed to encapsulate a variety of internal variability states, whose climate effects largely cancel out when considering the ensemble mean to capture the externally forced signal, provided the ensemble is large enough (Milinski et al., 2020).

Previous studies have shown that decadal prediction systems can skillfully predict the NA Ocean's variability for both SST and OHC (e.g. Keenlyside et al., 2008; Pohlmann et al., 2009; Robson et al., 2012; Mignot et al., 2016; Kröger et al., 2018; Borchert et al., 2018; Robson et al., 2018; Yeager et al., 2018; Bilbao et al., 2021; Volpi et al., 2021; Carmo-Costa et al., 2021; Polkova et al., 2023), as well as other related variables like the NAO (Athanasiadis et al., 2020; Smith et al., 2020) or the Atlantic Multidecadal Variability (AMV) (Doblas-Reyes et al., 2013; Volpi et al., 2017; Borchert et al., 2018; Delgado-Torres et al., 2022), and that initialization has a positive impact on the predictive skill. However, there are both qualitative and quantitative differences across decadal prediction systems when it comes to predictability time range, areas with significant predictive capacity, and magnitude of the associated skill. Several multi-model studies have shown how different model biases in the Labrador Sea, from near surface densities (Menary and Hermanson, 2018), the upper ocean mean stratification (Ortega et al., 2021; Kim et al., 2023a) or the local co-variability between temperature and salinity (Menary et al., 2015), can degrade important aspects of the North Atlantic decadal variability, including its predictability. Furthermore, model drifts and initial shocks have been shown to impact the quality of decadal climate predictions (Kröger et al., 2018; Polkova et al., 2019; Bilbao et al., 2021), although it remains unclear whether anomaly initialization methods, specifically designed to minimize such drifts, provide real predictive advantages over traditional full-field initialization approaches (Smith et al., 2013; Hazeleger et al., 2013; Volpi et al., 2017; Kröger et al., 2018; Polkova et al., 2023). Understanding the differences in skill across models, and in particular the factors that control and enhance the regional predictability, is essential to inform and improve the next generation of decadal prediction systems.

The concrete goal of this study is to assess the predictive skill of the upper 700m OHC in the North Atlantic using decadal prediction systems and historical simulations from CMIP6, exploring also the processes and methodological factors behind the inter-model differences. In particular, we investigate the relative role of external forcings in the predictive skill, and how it varies regionally. We also examine whether some skill limitations or improvements can be associated with specific methodological choices, such as the initialization strategy and model resolution considered. A special focus is placed on the Labrador Sea OHC, where models show important differences in predictive skill, to evaluate the impact of several local drivers and pre-conditioners on the skill. This paper is organized as follows: Section 2 describes the observational products, models and simulations used, the criteria for the final ensemble selection, as well as some data processing considerations; Sections 3.1, 3.2, 3.3 and 3.4 present

the results in four separate scientific blocks: (i) a multi-model evaluation of the upper OHC skill in the NA Ocean to assess the consistency of the results across models and identify outlier behaviors and regions of interest, (ii) a deeper investigation of the role of external forcings and long-term trends in the upper OHC skill in the Labrador Sea (identified in *i* as a region of interest for its large inter-model differences); (iii) an inter-model comparison of key Labrador Sea mean state model properties that could potentially condition the local OHC variability and skill; and (iv) an analysis of how those model properties affect the inferred predictive role of external forcings on Labrador Sea OHC variability, introducing some observational references to constrain the inter-model uncertainty. The final Section summarizes the main results and discusses them in light of previous studies.

2 Data and methods

This analysis considers both historical (named HIST hereafter) and DCPP component A (Boer et al., 2016) retrospective decadal prediction ensembles of the CMIP6 initiative to explore the effects of external forcings and internally generated variability on the observed OHC variability and the ability of current climate models to predict it. We will focus on the OHC in the upper 700m (referred to as OHC700 hereafter) and the main pre-conditioners and large-scale drivers of its regional variability and predictability, paying special interest to the major inter-model differences.

2.1 Climate model selection

The model selection was based on three criteria: (1) both the HIST and DCPP experiments were available via the Earth System Grid Federation (ESGF) portal for each model; (2) both the HIST and DCPP experiments were driven with the CMIP6 external forcings to ensure complete consistency in the forced signals; and (3) in both sets of experiments the relevant output variables for our analyses, such as 3D salinity (*so* in CMIP convention), 3D potential ocean temperature (*thetao*), 2D sea level pressure (*psl*), downward surface heat fluxes (*hfds*) and sea ice concentration (*siconc*), were available at monthly frequency for the period 1960-2014 (which is their overlap period). Also, except for two justified exceptions (details below), models with fewer than 10 ensemble members for HIST and/or DCPP were excluded. A total of 8 AOGCMs were retained based on the selection criteria. For models that provided more than 10 ensemble members, in either the HIST and DCPP experiments, only 10 members were retained to maximize the consistency across models. By default, we took members r1-10, except for EC-Earth3 historical simulations that we used 10 members performed at the BSC (i.e. r2,r7,r12,r17-22,r24). This ensemble size is the minimum that is recommended for the DCPP-A protocol in (Boer et al., 2016) and is the most common ensemble size across the models considered. Both HadGEM3-GC31-MM and MPI-ESM1-2-HR contributed with less than 10 ensemble members (4 HIST members and 5 DCPP members, respectively), but since both have comparatively higher horizontal resolution (0.25º and 0.4º, respectively) they were included to assess if there is any added value, either in process representation or predictive skill, when horizontal resolution is increased. More details on the models considered in this analysis and their characteristics can be read in Table 1.

2.2 Verification datasets

We used the EN4 version 2.2 ocean temperature and salinity objective analysis dataset based on optimal interpolation (Good et al., 2013) to evaluate the predicted OHC700 and the ocean stratification. Three ocean reanalyses - ECDA3.1 (Chang et al., 2013); ORAS4 (Balmaseda et al., 2013); ORAS5 (Zuo et al., 2019); the same used in Carmo-Costa et al. (2021) - were additionally considered and compared with EN4 to identify the regions with high and low OHC700 observational uncertainty (Figure A1).

To understand the processes driving local OHC700 skill we analysed additional variables, such as sea-level pressure, surface heat fluxes and sea-ice concentration. To determine how realistically the systems simulate these variables, we compared them with other observationally-based datasets. For the atmospheric variables we used the global atmospheric reanalysis ERA5 (Hersbach et al., 2020), as it provides a complete and physically coherent description of recent atmospheric variability that is constrained by observations. These include monthly sea-level pressure fields (necessary to compute the NAO) and net surface heat fluxes (derived from thermal radiation, surface solar radiation, surface sensible heat flux and surface latent heat flux). Finally, to evaluate the sea-ice concentration we used the monthly fields of HadISST.2.2.0.0 (Titchner and Rayner, 2014, hereinafter simply HadISST).

2.3 Data preprocessing

Data from both models and verification products were regridded to a common regular 1ºx1º resolution grid. All model outputs were regridded using the Earth System Model Evaluation Tool (ESMValTool; Righi et al., 2020) versions 2.4.0 to 2.7.0, which was particularly useful for its ability to process all models, experiments, start dates and variables in a consistent way. For other pre-processing tasks that were less computationally intensive, such as the calculation of yearly averages or the regridding of the ERA5 reference data, the Climate Data Operators tool version 1.9.10 (https://mpimet.mpg.de/cdo) was preferred. Additionally, we used ESMValTool to compute the OHC700 and potential density anomaly (σ - sigma; computed for the reference level of 1000m). The post-processed outputs were then analysed with both the s2dverification/s2dv package (Manubens et al., 2018; Guemas et al., 2019) for R software and python scripts that have been developed purposely for this research. Both the NAO and the linear regression analysis were also computed with s2dverification/s2dv.

2.4 Forecast verification

To evaluate the forecast quality of the models we used the anomaly correlation coefficient (ACC). The statistical significance of ACC differences was assessed following the methodology proposed by Siegert et al. (2017), a statistical test developed for cases where competing forecasting systems are strongly correlated with one another.

An important aspect to consider when comparing predictive skill between a DCPP experiment and its HIST counterpart is the selection of a common period for forecast evaluation, to ensure that differences in skill only arise from the effect of initialization (as prediction skill can be sensitive to the evaluation period). Our evaluation period is fixed and starts in 1970 - the first year for which the DCPP ensemble provides predictions for the full forecast range (1st to 10th year) - and finishes in

2014, which is the last year covered by the HIST ensemble. Linear trends in our analysis were also computed for this same period.

Not all models in this analysis were initialised in the same month. One model was initialised in the first of October (NorCPM1), several in the first of November (CMCC-CM2-SR5, EC-Earth3, HadGEM3-GC31-MM, MPI-ESM1-2-HR and MRI-ESM2-0) and the others in the first of January (CanESM5 and IPSL-CM6A-LR). Therefore, for practical reasons, in all models we computed all forecast years (FY1-10) January through December, discarding the first months from those models initialised in October and November. Additionally, we computed the boreal winter mean (defined from December to February, referred to as DJF hereafter), which is important for some of the processes and drivers investigated (like the NAO). The forecast winters were numbered according to their January and February forecast years, which means that, for example, DJF2 refers to the winter that includes the December month of FY1 but months January and February of FY2. We discarded DJF1 from all analyses since some systems do not fully predict the first winter (as it requires December of FY0).

3 Results

3.1 Multi-model OHC700 skill assessment

We first evaluate the ACC for OHC700 in all the prediction systems for three different forecast times (years 2, 5 and 10), as well as in all the historical ensembles. Overall, all decadal prediction systems show positive correlations for most of the NA at all the different forecast ranges (Figure 1, columns 1-3), with higher correlations typically taking place in the Labrador Sea and along the Eastern flank of the basin, and negative correlations developing in a region located east of the Grand Banks (EBG; approx. 40-55 ºN and 40-25 ºW, with small regional differences across models). We note that over the EBG region, the ocean reanalyses and EN4 show the highest discrepancies in terms of OHC variability (Figure A1), and therefore the associated skill scores are expected to be more uncertain and should be interpreted with caution. We also note that no systematic overall improvement at any forecast time is observed for systems based on full field initialization compared to those using anomaly initialization, and vice versa (first 4 rows vs. last 4 rows in Figure 1). The ACC patterns for HIST are generally close to those in the predictions, although with a tendency for more widespread negative correlations and lower positive correlation values than in the predictions. The largest added value of initialization, as indicated by the ACC differences between the DCPP and HIST ensembles, is found predominantly in the Subpolar Gyre region (Figure A2). Residual correlations, introduced by (Smith et al., 2019), help to more clearly identify regions where initialization is beneficial for prediction. These correlations (Figure A3 reveal another area with a strong added value of initialization in the Eastern North Atlantic. However, this result should be interpreted with caution, as residual correlations assume that models accurately represent the forced signals in observations—an assumption that may not hold in regions where the HIST ensemble exhibits high inter-model differences.

We now turn our attention to some specific cases of distinct individual model behaviour in Figure 1. While in most models ACC values tend to be highest in FY2 and usually decrease as the FY progresses, as expected due to the effect of initialization, this is not the case for IPSL-CM6A-LR and CanESM5. In both models ACC is higher in FY5 and even FY10 than in FY2 over the Labrador Sea (LS) and the EGB region. The comparatively lower skill in FY2 that in subsequent forecast years for

IPSL-CM6A-LR and CanESM5 might be caused by a strong initialization adjustment, as their historical ensembles show comparatively higher ACC values than the DCPP at FY2. Another system showing a rapid loss of skill in the LS and EGB regions is NorCPM1, where negative correlations emerge by FY5 and FY10. In this case, it might reflect a deficiency in the representation of the forced signals, which could be related to a reported problem in the transient land use specification in North America, with downstream impacts in the Subpolar North Atlantic area (Bethke et al., 2021; Passos et al., 2023). Its HIST ensemble has a large area of negative skill values over the LS and its surroundings. Interestingly, in this same region NorCPM1 predictions show the highest levels of skill at FY2, which suggests that initialization can temporarily correct the errors in the land-use forcing.

Figure 2 describes the inter-model differences in ACC shown in Figure 1, as diagnosed by the standard deviation of the ACC values across models. The HIST experiments have higher ACC spread than the DCPP experiments over most of the NA at all forecast years. The largest standard deviation values (and thereby inter-model differences), are found for HIST along the Eastern North Atlantic (up to 0.6) and in the LS (up to 0.4). In the DCPP experiments, the inter-model spread tends to change with forecast year, without much spatial consistency in terms of the regions with the largest standard deviations. The LS (red rectangle in Figure 2; 60-30ºW and 45-65ºN.) emerges as a region in which inter-model differences in skill are prominent at all forecast times. We note that the selected box extends into the Irminger Sea, that also shows important inter-model spread. Other studies have referred to this same area as the western Subpolar Gyre (Hermanson et al., 2014). We also note that this is a characteristic region of deep vertical mixing, with common precursors and drivers whose representation may vary across models, and could explain the inter-model spread. Hence, in the rest of the study we will focus on this region to understand its inter-model differences in OHC skill.

3.2 Role of forcings and long-term trends in Labrador Sea OHC skill

To better understand the differences in skill, the predicted and the observed evolution of LS OHC700 anomalies is shown in Figure 3. At FY2 and FY5, all systems but CanESM5 predict the observed evolution reasonably well, characterized by a very weak cooling trend until the mid-90s, after which a warming trends starts to unfold. CanESM5's long-term trend is characterized by a cooling, completely failing to represent the warming after the 90s. This could be related to the use of ORAS5 for initialization (Sospedra-Alfonso et al., 2021), which has been reported to have non-stationary trends in the region (Tietsche et al., 2020). At longer forecast times (FY10), all models except CanESM5 and NorCPM1 simulate a long-term warming trend of similar amplitude to the observed one, although none of the models captures well the relative cooling between 1990-1995.

Interestingly, in the HIST ensemble only two models, IPSL-CM6A-LR and CanESM5, simulate a clear warming trend consistent with the observed one. The other models show a rather flat evolution and NorCMP1 shows a cooling trend. We also note that none of the HIST ensembles simulate the cooling until the mid-90s nor the subsequent rapid warming that were partly captured by the DCPP experiments, supporting a key role of initialization in the decadal variability around the trend.

Figure 4 shows that the relationship between the OHC700 trends (as derived for the period 1970-2014, see Section 2.4) and the OHC700 skill in the LS is largely linear across models. In other words, models with stronger OHC700 trends in the LS tend to have higher OHC700 skill in this region, which is particularly evident in the HIST ensemble and the first forecast

years of the DCPP ensemble, although with some notable differences. While for HIST, all the models show a wide range in the magnitudes of the simulated trends, in the first forecast years of the DCPP ensemble all models predict similar trends to the observed one, except for CanESM5 which has been previously mentioned as an outlier. This clear correction of the predicted trend via initialization can imply that: (1) the observed LS trend is only driven by internal variability processes; or (2) external forcings contribute to the trend but require realistic background climate conditions — achieved through initialization — to represent it accurately. Interestingly, predicting well the trend does not always lead to high levels of OHC700 skill, as noted for, e.g., IPSL-CM6A-LR at FY2 in Figure 4.

To further investigate the impact of the long-term trends on the OHC700 skill in the LS, Figure 5 portrays the ACC values as a function of FY when both DCPP and the observed data are linearly detrended (dashed blue line), and compares them with the skill for the original time-series (solid blue line). In all models, except for CanESM5, the forecast skill systematically decreases when the trend is removed, even though the drop in skill is not always significant with respect to the undetrended ACC values (red crosses in Figure 5). This confirms that an important part of the skill comes from the representation of the trend. Figure 5 also shows the forecast skill of the HIST ensemble, which compared with the DCPP skill can inform us about the predictive role of the forcings. The results are largely model-dependent. In some systems, HIST and DCPP have similar ACC values that are only significantly different in the first FYs, which suggests a predominantly forced origin of the skill. Other models, like MRI-ESM2-0, HadGEM3-GC31-MM and CMCC-CM2-SR5, show high and significant ACC values for DCPP, while for HIST the ACC values are indistinguishable from zero. The interpretation of these latter systems is more complex, as the high predictive value of initialization could imply that internal variability is the dominant factor leading to the OHC700 skill, but it is also possible that the corresponding HIST ensembles simulate an unrealistic externally forced variability that is largely corrected via initialization. It is also possible that external forcings exert only a prominent role in OHC predictability for some specific areas within the wide Labrador Sea box considered. Indeed, all models but NorCPM1 show positive skill for their historical ensemble in the westernmost part of the region, and poorer skill in its easternmost side (Figure 1).

Figure 5 thus illustrates how the large uncertainties in the representation of the forced signals, together with the initialization shocks in some of the systems (CanESM5, EC-Earth3, IPSL-CM6A-LR) prevent us from learning about the true origin of the LS OHC700 predictability. The underlying problem is that we do not know how much of the observed variability is actually driven by the forcings. In the next two sections (3.3 and 3.4) we will explore (i) how different precursors and drivers of LS decadal variability are represented across models and experiments, to ultimately investigate (ii) whether they can explain some of the inter-model differences in the forced LS OHC700 predictive skill.

3.3 Evaluation of main preconditioners and drivers of LS OHC700 variability across models

In this section we explore the underlying differences across models of two important factors controlling Labrador Sea temperature variability: (1) LS stratification and (2) the surface atmospheric forcing. The former is a preconditioning factor for the occurrence of deep convection in the region, whereas the latter is a direct driver of convection and OHC variability via its influence on local air-sea heat fluxes. We note, however, that these factors can also interact with each other. For instance, in strongly stratified models where deep convection is suppressed, atmospheric forcing may instead lead to sea ice forma-

tion. In the following, we will evaluate how models simulate these important processes, and whether they are improved via initialisation.

3.3.1 The preconditioning role of density stratification

It is well known that the LS is an important region where oceanic processes, such as deep ocean convection, can drive large-scale ocean temperature changes (Robson et al., 2016; Ortega et al., 2021). It is, however, less clear if these processes influence the local OHC skill, or if OHC persistence is the dominant factor (Buckley et al., 2019). Some prediction systems, like the one based on EC-Earth3, show high OHC predictive skill in the NA even after LS convection collapses due to initialization effects (Bilbao et al., 2021), which suggests that other processes besides the local deep mixing might also be relevant.

In the LS, deep convection takes place in winter (Yashayaev and Loder, 2016), when the local cooling exerted by the atmosphere can be strong enough to overcome the local density stratification, which acts as a preconditioner. Important model biases in density stratification can therefore potentially mitigate and even suppress deep ocean convection and in this way limit the forecast skill, especially in anomaly initialised systems in which potential model biases are not corrected during initialization.

Figure 6 shows the climatological wintertime (DJF) potential density profiles for the LS area 6) in DCPP and HIST. The HIST panel, which describes the intrinsic mean-model biases, shows that IPSL-CM6A-LR, EC-Earth3 and especially CanESM5 have overly stratified LS densities, as compared to EN4, while NorCPM1 stands out as a model with virtually no LS density stratification. These are two opposite problems that interestingly seem to arise from biases in the salinity profile (bottom panel of Figure A4). When looking into the DCPP experiments, NorCPM1 still shows the overly weak LS stratification. In contrast, full-field initialization seems to efficiently correct the strong stratification problems, especially in CanESM5, although in EC-Earth3 stratification is degraded in DJF10 compared to HIST, likely due to the initialization shock reported in Bilbao et al. (2021).

We now revisit the potential density profiles but focusing on how differently the models represent the temporal variations at different levels, as these can reveal other important model biases affecting the vertical mixing. NorCPM1 and IPSL-CM6A-LR portray the largest differences with respect to EN4 for both DCPP and HIST (bottom panel of Figure 6), in particular near the surface where the variance is higher due to the exchanges with the atmosphere. NorCPM1 shows substantially weaker variability at the surface, while IPSL-CM6A-LR shows the largest variability. This might derive from their radically different mean winter stratification (top panel of Figure 6): In NorCPM1 the very weak stratification ensures a rather sustained mixing, which damps the year-to-year variability. In contrast, in IPSL-CM6A-LR, stratification is relatively strong, favoring a much too intermittent mixing. There is no clear benefit from initialization in the variability profiles for most models. In fact, initializing the models seems to worsen the density variability for CanESM5 in DJF2-DJF5, which can be again linked to the non-stationarity errors inherited from ORAS5.

In the next subsection we will explore whether the differences in stratification can condition the local forcing from the atmosphere.

3.3.2 The North Atlantic Oscillation as a key driver of LS variability

Many studies have highlighted the key driving role of the NAO on the interannual variability of LS temperature, salinity and convection (e.g., Eden and Jung, 2001; Guemas and Salas, 2008; Ortega et al., 2012; Yashayaev and Loder, 2016), and through it, on the AMOC, but, to our knowledge, no study to date has explored whether and how structural model differences in the representation of the NAO affect the local air-sea heat exchanges.

Figures 7 and 8 show the NAO pattern (defined as the first EOF of sea level pressure in DJF) for the HIST and the DCPP experiments, respectively. As expected, the low-pressure system (also known as Icelandic Low; IL) tends to be centred around Iceland, and the high-pressure system (also called Azores High; AH) is centred between Azores and the western border of the Iberian Peninsula. There are some notable differences across models and experiments. In the HIST experiments (Figure 7) both the AH and IL show substantial variations in their location across models and also across members (indicated by the crosses). Overall, the AH tends to be more located near the Azores Archipelago, although some individual model members, including all NorCPM1 ones, develop their maxima near the Iberian Peninsula.

Important differences across models are also found in terms of the IL location for both types of experiments. CanESM5 (more obvious in HIST), CMCC-CM2-SR5 and NorCPM1 tend to have the IL located further to the East (i.e., over the Norwegian Sea and Scandinavia), much like the NAO structure of ERA5 for the study period of 1970-2014 (Figure A6). The other models have their centres of action over Iceland and Greenland, which is more in line with the traditional NAO definition (Hurrell, 1995).

There seems to be an overall agreement between the NAO patterns in the HIST and DCPP ensembles (Figure 8). In the DCPP experiments, the centres of action of the ensemble mean remain largely unchanged with forecast time (indicated by the circles of increasing size). This suggests that full-field initialization, despite improving the representation of the SST patterns driving the NAO (e.g. Gastineau and Frankignoul, 2015), does not correct the position of its simulated centres of action, which are located too far to the east in models like CMCC-CM2-SR5 and CanESM5.

The relative position between the AH and IL centres of action can critically condition how the NAO affects the surface winds, whose speed is proportional to the local gradient in sea level pressure. This can be crucial in the Labrador Sea, where the surface winds promote deep ocean convection by cooling the surface. Models like NorCPM1 or CMCC-CM2-SR5, in which both centres of action are placed far from the Labrador Sea, shifting the maximum sea level pressure towards the east, might therefore induce a weaker local forcing. We now investigate whether this is the case by computing the linear regression of the NAO index with the surface heat fluxes (Figure 9), as represented by the CMIP6 variable *hfds*. In the HIST experiments (rightmost column), all models show that the NAO exerts a strong cooling in the Labrador and Irminger Seas, except in CanESM5, where both regions are unrealistically covered by sea ice (Figure A7). Interestingly, the HIST panel additionally suggests that having the IL centre displaced to the east, like for NorCPM1 and CMCC-CM2-SR5, does not necessarily lead to a lack of surface forcing in the LS. This result suggests that other factors influencing the local heat loss are at play.

For the DCPP ensemble, the regression maps (Figure 9) show a clear beneficial effect of initialization in the representation of the NAO's surface forcing, especially over the LS. In that region, all models show a more consistent picture at DJF2, and

a better agreement with the equivalent regressions in ERA5 (Figure A6) suggesting that having more realistic conditions in stratification, sea-ice or both does help to improve the NAO's influence on the local OHC (e.g., via improved vertical mixing), even in cases where its centers of action are displaced compared to ERA5 (e.g., CMCC-CM2-SR5). As the forecast time progresses, differences start to emerge, particularly in the systems that are full-field initialised (e.g., CanESM5, EC-Earth3, CMCC-CM2-SR5) following the development of the intrinsic model biases. Indeed, full-field initialization not only helps to simulate a more realistic forcing of the NAO, it also critically improves the climatological surface heat fluxes in winter (Figure A5 compared to Figure A6), mean-state improvements that are very clear in the LS in DJF2 for CanESM5, CMCC-CM2-SR5 and EC-Earth3. These improvements are less noticeable for HadGEM3-GC31-MM, which is also full-field initialized, because this model had a more realistic background mean state density stratification, as evidenced in Figure 6 for its HIST run. Figure A5 also distinguishes NorCPM1 as a model with overly large climatological heat loses into the atmosphere in both the LS and EGB as compared to the other models and ERA5.

To help identify the specific regions where the NAO introduces larger differences across models in terms of local surface heat fluxes, Figure 10 (top row) shows the standard deviation in model space for the regression coefficients shown in Figure 9. It clearly illustrates that the major differences occur over the LS, especially on its western side, thus supporting that the representation of the NAO and its forcing may contribute to the differences in OHC700 skill across models (Figure 2). This is true for both sets of experiments, although the area of high standard deviation values is larger in HIST. The differences across models are reduced with initialization and become more prominent in the LS as forecast time progresses, and by DJF10 they remain geographically more confined than for the HIST experiment.

Because winter heat fluxes are not exclusively linked to the NAO, the differences across models in terms of climatological winter surface heat fluxes alone are plotted in Figure 10's middle row. Strong multi-model differences are also evident, with much higher standard deviation values. These are not only limited to the LS, which clearly stands out as the region with the highest inter-model spread, but are also quite large over the EGB region.

Considering that sea ice can act as a barrier that shields the ocean from the atmospheric influence, and in this way condition the climatological heat fluxes, the inter-model spread of the winter sea-ice concentration (when it reaches its maximum extent) is also presented in the bottom row of Figure 10. While in HIST and DJF10 there is a large spread in LS climatological sea ice, which can be mostly associated to CanESM5 and EC-Earth3 (Figure A7), in the forecast winters DJF2 and DJF5 the differences are confined to a narrow band at the westernmost side of the LS. This is also where the surface heat flux regressions onto the NAO and the climatological surface heat fluxes showed the largest intermodel spread. Therefore, it would seem that all the three model properties are intricately related in that region.

3.4 Understanding uncertainties in the externally forced LS OHC700 variability and predictability

This last section seeks to narrow down the large uncertainties identified in the LS OHC700 externally forced signal, by contrasting the HIST simulations against observationally-based values for the previously analysed key physical properties (i.e., stratification, NAO regression, surface heat fluxes and sea ice concentration). To this end, a set of scatter plots was assembled in Figure 11.

We find a strong linear relationship between the forced OHC700 skill and the stratification index, with stronger stratification linked to higher skill. This result is robust for different definitions of the stratification index considered (not shown). A possible interpretation of this linear relationship is that stronger mean stratification limits the occurrence of deep convection events, especially those triggered by internal climate variability processes (which in HIST runs cannot be in phase with the observations), allowing for a better capture of the long-term trends. However, it is important to note that the models with the largest forced OHC700 skill also largely overestimate the local stratification when compared to an observational reference, which raises questions about their realism.

The relationship between the OHC700 skill and the climatological winter surface heat fluxes (*hfds*) in the LS (Figure 11c) is also highly linear. In this case, however, both variables exhibit an inverse relationship: models like NorCPM1 or MRI-ESM2-0 that have stronger climatological surface heat fluxes in the LS (i.e., that lose more heat to the atmosphere) tend to have lower ACC values for OHC700, and vice versa. One potential explanation for this relationship is that with stronger heat fluxes the local stratification can be overcome more easily, which therefore allows for a higher presence of spurious unforced signals that degrade the agreement with the observations (i.e., lower the ACC value). Interestingly, even though higher ACC values are linked to weaker surface heat forcings, the observed ERA-5 climatologies suggest that the models with the highest forced skill are not particularly realistic. It should be noted, however, that ERA-5 does not include all of the air-sea ice fluxes that are included in the HIST fluxes, and might be important at the western side of the Labrador Sea.

For the two other preconditioners identified in section 3.3.2 (i.e., the local NAO surface forcing and the climatological sea ice conditions) we do not find a clear linear relationship with the forced OHC700 LS skill. Despite this, CanESM (the model with the highest ACC values) is identified in both cases as a clear outlier when compared with observation-based references.

All the above results thus suggest that high ACC values in some of the historical ensembles are not necessarily indicative of good model performance. The underlying issue is that the true split between the forced and the internally generated variability in the real world is unknown, which hinders the identification of the models that simulate the forced signal better. Interestingly, the observation-based references included in the scatter plots are generally close to the multi-model mean value, supporting its standard use to derive our best estimate of the real forced signal. This multi-model mean has a forced OHC700 skill in the LS of $\sim$0.4, which would imply a significant but not dominant contribution of the external forcings to Labrador Sea OHC700 variability (as it would explain around 16% of the total variance).

4 Conclusions and Discussion

In this study, the predictive skill of the North Atlantic upper Ocean Heat Content has been explored in a multi-model context, using CMIP6 ensembles of historical and decadal climate prediction experiments from eight different models. By analysing both ensembles of experiments it has been possible to investigate how and to what extent the external forcings contribute to the regional predictability of the OHC, assessing also the benefits of initialization. The bulk of the analysis has been delimited to the Labrador Sea region, where important skill differences across models were found. To further understand these inter-model differences, we have explored whether they can be linked to the capability of the underlying models to represent key ocean-

atmosphere processes and properties that are tightly connected to the local OHC700 variability, such as the preconditioning role of density stratification and the NAO influence on the surface heat fluxes.

The main findings of the paper are summarized as follow:

- Initialised decadal predictions largely agree on the regions with high predictive capacity for the OHC, which mostly concentrate on the Labrador Sea region and the eastern flank of the North Atlantic. All of them also show a region with negative skill located east of the Grand Banks, albeit with important differences regarding the exact location and extension of the negative ACC values, which largely varies across the models and experiment types. It remains unclear how much of this low skill is attributable to the large local observational uncertainties, which affect both the verification datasets and the quality of the initial conditions, as these latter are derived from assimilated observations. From these three regions, the largest inter-model differences in terms of predictive spread occur in the Labrador Sea, where some models experience initial shocks, as identified by Polkova et al. (2023), degrading the skill some years after initialization.

- In the Labrador Sea region, no clear picture emerges from the multi-model ensemble of how much predictive capacity for the OHC arises from external forcings, as large inter-model differences in ACC are found for the OHC of the HIST experiments. The added predictive value of initialisation, determined as the difference in skill between DCPP and HIST ensembles, is also highly variable across models. This model-dependence of the results highlights the importance of using multi-model approaches, as analyses focused on individual models, like the one in Carmo-Costa et al. (2021), can potentially lead to misleading generalizations.

- In the HIST experiments, we have identified a strong linear relationship between the skill for Labrador Sea OHC and the local density stratification, as well as a strong inverse linear relationship between the same skill and the climatological local surface heat fluxes. Since both stronger stratification and weaker surface heat fluxes suppress vertical mixing, we interpret that models with higher OHC skill are those where deep mixing occurs only sporadically, thereby reducing the influence of spurious signals from internal variability, which tend to lower correlation values. Interestingly, Hegerl et al. (2021) previously established a connection between density stratification in the North Atlantic subpolar gyre and local prediction skill for SST in models, showing that a more realistic stratification enhances skill levels. However, it is challenging to directly compare their findings with ours, as their analysis focused on a broader region, initialized predictions, and assessed absolute stratification errors without considering their directionality.

- The HIST experiments with higher ACC for the Labrador Sea OHC also have larger biases in the mean state stratification and heat fluxes, which questions their realism. The multi-model mean of the HIST experiments compares particularly well with observations, and is likely to provide a more realistic estimate of the predictability attributable to the forcings, which according to the multi-model mean would account for $\sim$16% of the total OHC variance in the Labrador Sea. We note that this number is roughly consistent with the percentage of Atlantic Multidecadal variability (AMV) accounted for by external forcings from 1870 to 2012 in the analysis of (Qin et al., 2020), which is derived from observations. Even if both quantities, the Labrador Sea OHC and the AMV, represent different domains and are derived from different

variables, they are linked physically, as Labrador Sea OHC is strongly linked to local deep mixing, which is an important driver of the AMOC, and through it, the AMV (Knight et al., 2005).

- Our multi-model DCPP ensemble includes 4 systems using anomaly initialization, and 4 systems using full-field initialization, which has allowed us to assess their relative merits. We have found that, overall, full-field initialization helps improving the representation of the selected key mean model features in the first forecast years, including the background stratification and the surface forcing from the NAO, but it does not necessarily lead to systematic improvements in Labrador Sea OHC skill, as already found in previous studies for the North Atlantic (Hazeleger et al., 2013; Volpi et al., 2017). No systematic benefit of anomaly initialization has been identified either, although for the case of NorCPM1 we have found significant OHC skill along the full forecast, despite an overly weak mean stratification and some reported local errors in the forced signals.

- Regarding the impact of enhanced resolution, neither of the two systems with eddy-permitting ocean components (HadGEM3-GC31-MM and MPI-ESM1-2-HR) show superior performance in terms of upper OHC skill in the Labrador Sea compared to the other coarser resolution models, with CMCC-CM2-SR5, EC-Earth3 and MRI-ESM2-0 showing very similar skill values at all FYs. This means that no particular benefit is obtained from the larger computing costs incurred by these higher resolutions, at least not for the subpolar latitudes in these DCPP experiments. It is possible, however, that the benefits of the higher resolution have been partly masked by the reduced ensemble sizes available for those models, as it has been previously shown that a larger ensemble size has a positive impact on the North Atlantic skill (Delgado-Torres et al., 2022; Athanasiadis et al., 2020). It is also possible that achieving significant skill improvements requires higher resolutions than those considered in this study. In fact, the first decadal predictions using an eddy-resolving ocean model, performed with CESM1.3 (Yeager et al., 2023; Kim et al., 2023b), demonstrated notable and widespread skill improvements compared to their low-resolution counterparts, although no real improvements were found in the North Atlantic, likely due to local issues in the initial conditions.

This study has linked the differences in upper OHC skill to different mean state biases across models, providing insights in relevant aspects of model fidelity that can be considered to guide the development phase of future climate prediction systems. A deeper fundamental understanding of the key sources of OHC predictive skill could be achieved by performing more holistic approaches, including heat budget analyses and the investigation of advective processes (similar to the propagation mechanisms described in Ortega et al. (2015) and Langehaug et al. (2022)), which are beyond the scope of this study. Novel approaches are also needed to cleanly disentangle the relative contributions from external forcings and internal variability to the predictive skill, as the added predictive value of initialization can arise from internal processes as well as a better representation of the forced response.

Code availability. All code developed for this study was based on ESMValTool, CDO, R or python. Scripts can be made available by the main author upon reasonable request.

Data availability. The CMIP6 simulations are available through the Earth System Grid Federation (https://esgf-data.dkrz.de/projects/esgf-dkrz/). EN4 version 4.2.2 can be found at www.metoffice.gov.uk/hadobs/en4/download-en4-2-2.html; we used the analyses files produced with the bias correction method from Gouretski and Reseghetti (2010). ERA5 can be downloaded from https://cds.climate.copernicus.eu/datasets/reanalysis-era5-complete?tab=overview and HadISST version 2.2.0.0 is available at https://www.metoffice.gov.uk/hadobs/hadisst2/.

Table 1. Summary of key features in the AOGCMs used in this study.

Dataset Name:	CanESM5	CMCC-CM2-SR5	EC-Earth3	HadGEM3-GC31-MM	IPSL-CM6A-LR	MPI-ESM1-2-HR	MRI-ESM2-0	NorCPM1
Ocean Model	CanNEMO	NEMO 3.6	NEMO 3.6	Global Ocean 6	NEMO 3.6	MPIOM 1.6.2	MRI.COM 4	BLOM
Ocean Grid	ORCA1	ORCA1	ORCA1	ORCA025	ORCA1	TP04	(tripolar)	NCAR's gx1v6
Horizontal Resolution	1°	1°	1°	0.25°	1°	0.4°	1x0.5°	1°
Vertical Levels	45	50	75	75	75	40	61	53
Ocean Initialization	ERSSTv3, OISST (SST), ORAS5 (T,S)	CHOR, CGLORSv7 reanalyses	ORAS5 (SST,SSS), EN4 (T,S)	Met Office Statistical Reanalysis (T,S)	ERSSTv3 (SST), Friedman et al. (2017) (SSS)	ORAS4 (T,S)	Ishii et al. (2017) (T,S) (down to 3000 m)	HadISST2.1, OISSTv2 (SST), EN4 (T,S)
Initialization Method	Full field (via nudging)	Full field	Full field (via nudging)	Full field (via nudging)	Anomaly (via nudging)	Anomaly (via nudging)	Anomaly (via IAU[a])	Anomaly (by EnKF assimilation)
References	(Swart et al., 2019)	(Cherchi et al., 2019; Nicolì et al., 2022)	(Bilbao et al., 2021; Döscher et al., 2021)	(Sellar et al., 2020; Kay et al., 2022)	(Bonnet et al., 2021)	(Müller et al., 2018; Li et al., 2019)	(Yukimoto et al., 2019)	(Bethke et al., 2021)
HIST members	r(1-10)i1p2f1	r(2-11)i1p2f1	r(2,7,12,17-22,24)i1p1f1	r(1-4)i1p1f3	r(1-10)i1p1f1	r(1-5)i1p1f1	r(1-10)i1p1f1	r(1-10)i1p1f1
DCPP members	r(1-10)i1p2f1	r(1-10)i1p1f1	r(1-10)i4p1f1	r(1-4)i1p1f2	r(1-10)i1p1f1	r(1-5)i1p1f1	r(1-10)i1p1f1	r(1-10)i1p1f1

[a] IAU - Incremental Analysis Updates

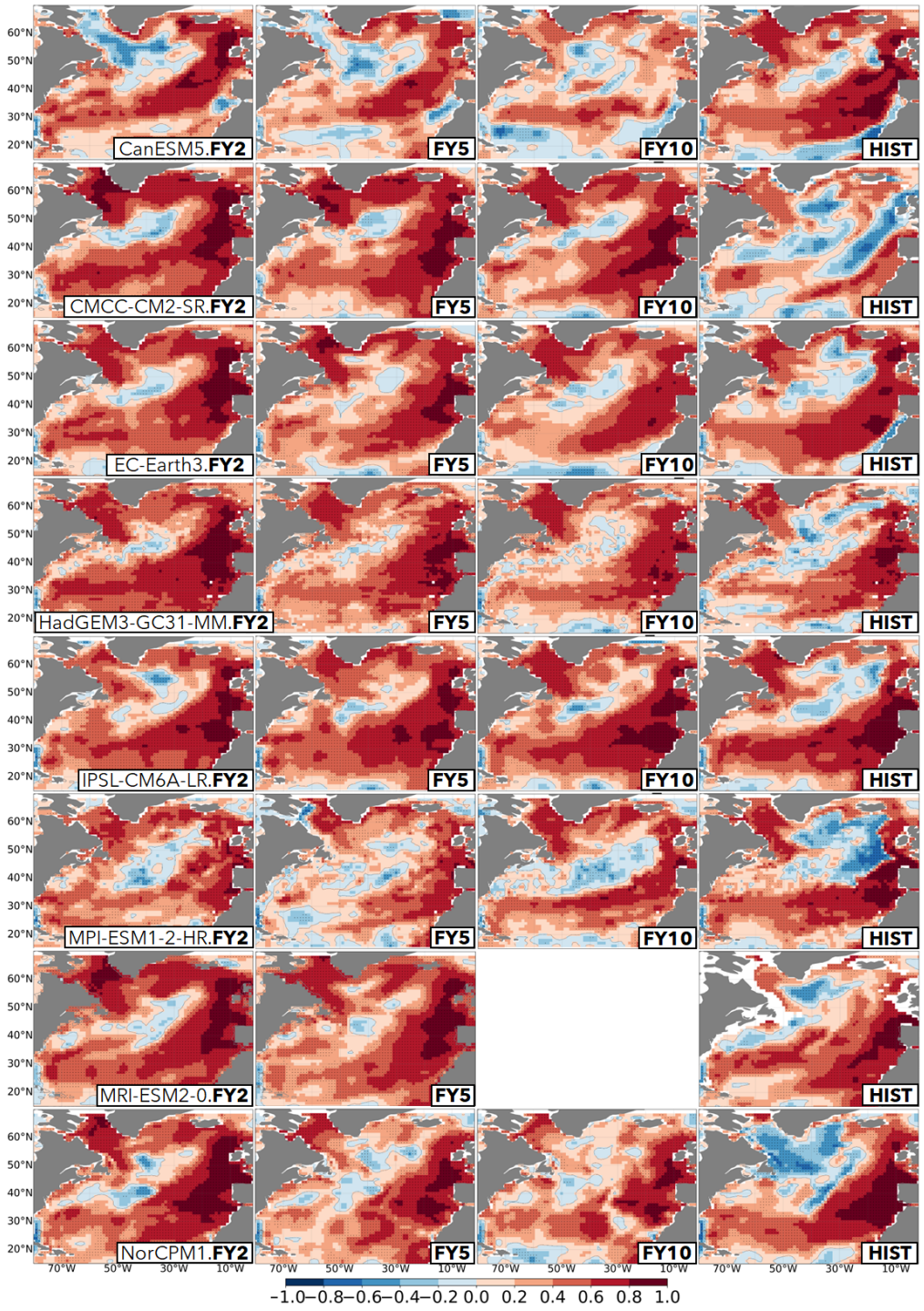

Figure 1. ACC maps for the OHC700 in the DCPP (forecast years 2, 5 and 10; columns 1-3, respectively) and HIST ensembles (column 4). Stippling indicates cells with correlation values statistically significant at the 95% confidence level. All ACC values are evaluated against EN4 for the period 1970-2014. Each row shows the results for a different model.

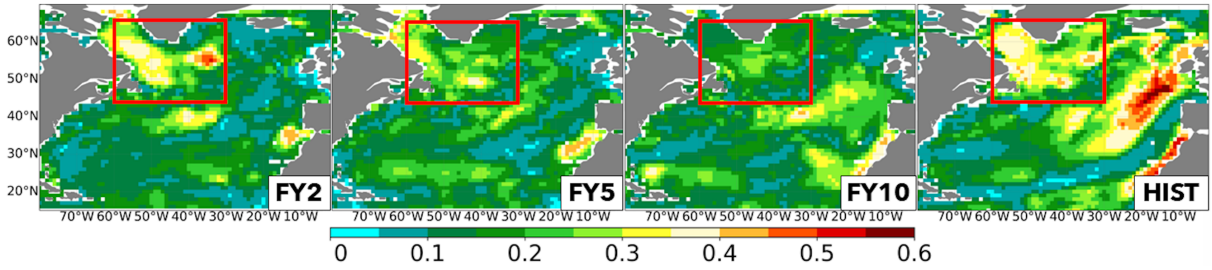

Figure 2. Standard deviation across models of the ACC values for OHC700 in DCPP (forecast years 2, 5 and 10; columns 1-3, respectively) and HIST ensembles (column 4). The red box encloses the Labrador Sea region, chosen to compute all area-weighted averaged mentioned hereinafter, with boundary coordinates 60-30ºW and 45-65ºN.

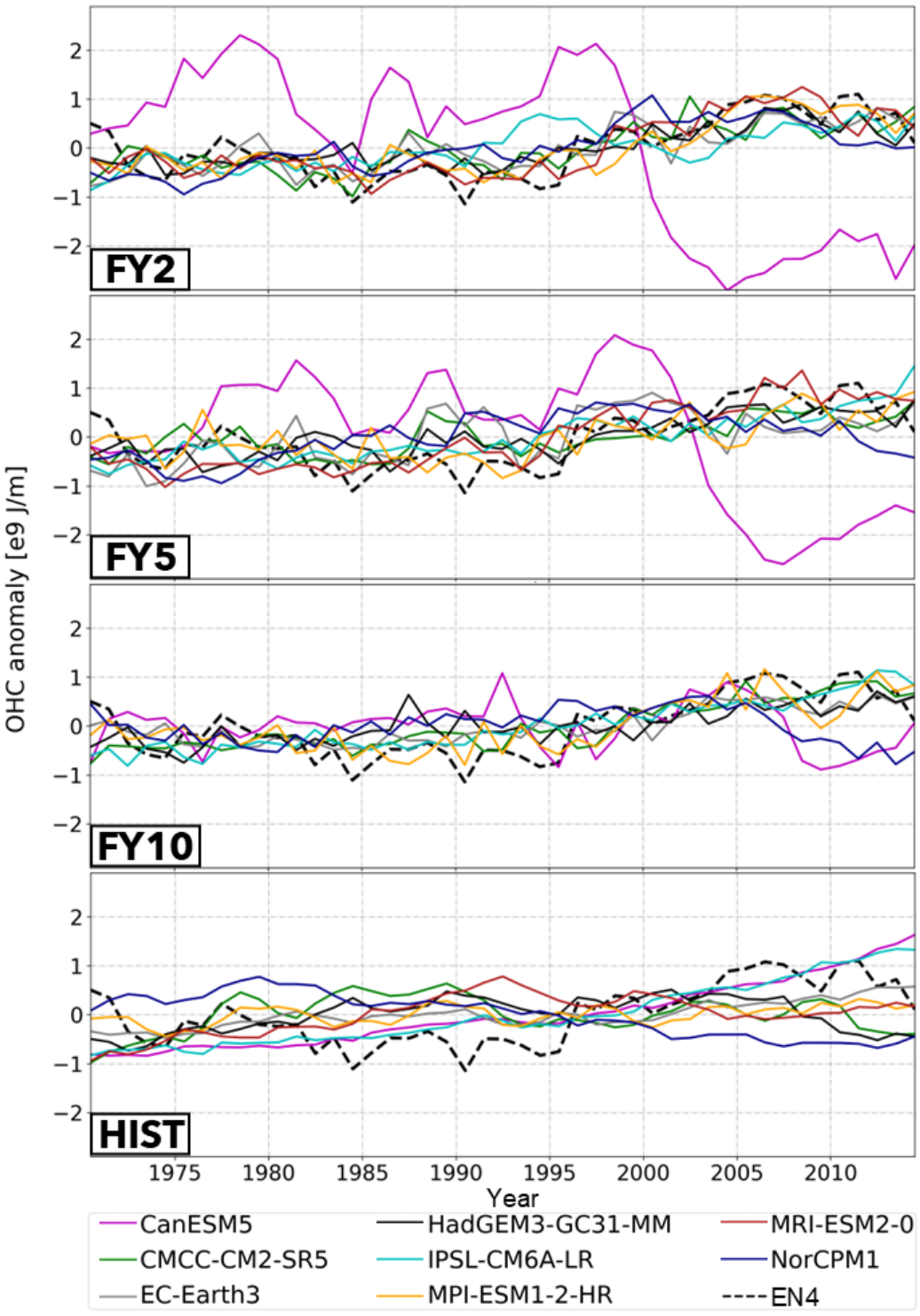

Figure 3. Timeseries of the spatially averaged OHC700 anomalies in the Labrador Sea region (red box in Figure 2), fo the DCPP (forecast years 2, 5 and 10) and HIST ensembles. The corresponding time series for EN4 observations is added as a dashed line.

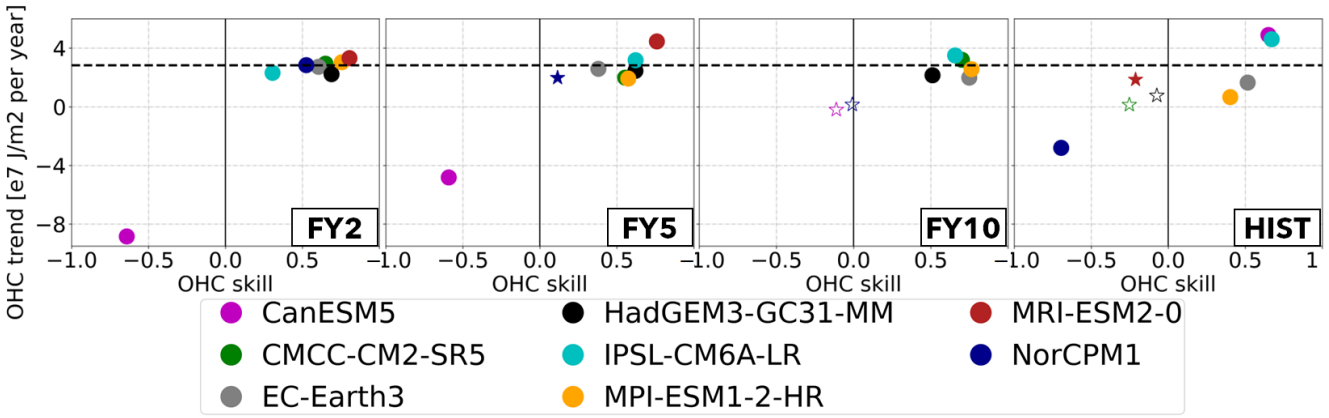

Figure 4. Scatter-plot of the relationship between the skill of OHC in the Labrador Sea region (red box in Figure 2) and the local OHC700 trend in both the DCPP (forecast years 2,5 and 10; columns 1-3, respectively) and HIST ensembles (column 4), all based on yearly averages. All trends were computed for the period of interest 1970-2014 (see Section 2.4 for more information). Stars represent non-significant correlation values at the 95% confidence level. Empty symbols represent non-significant trend values, at the 95% confidence level. The dashed black horizontal line represents the trends for EN4 observations.

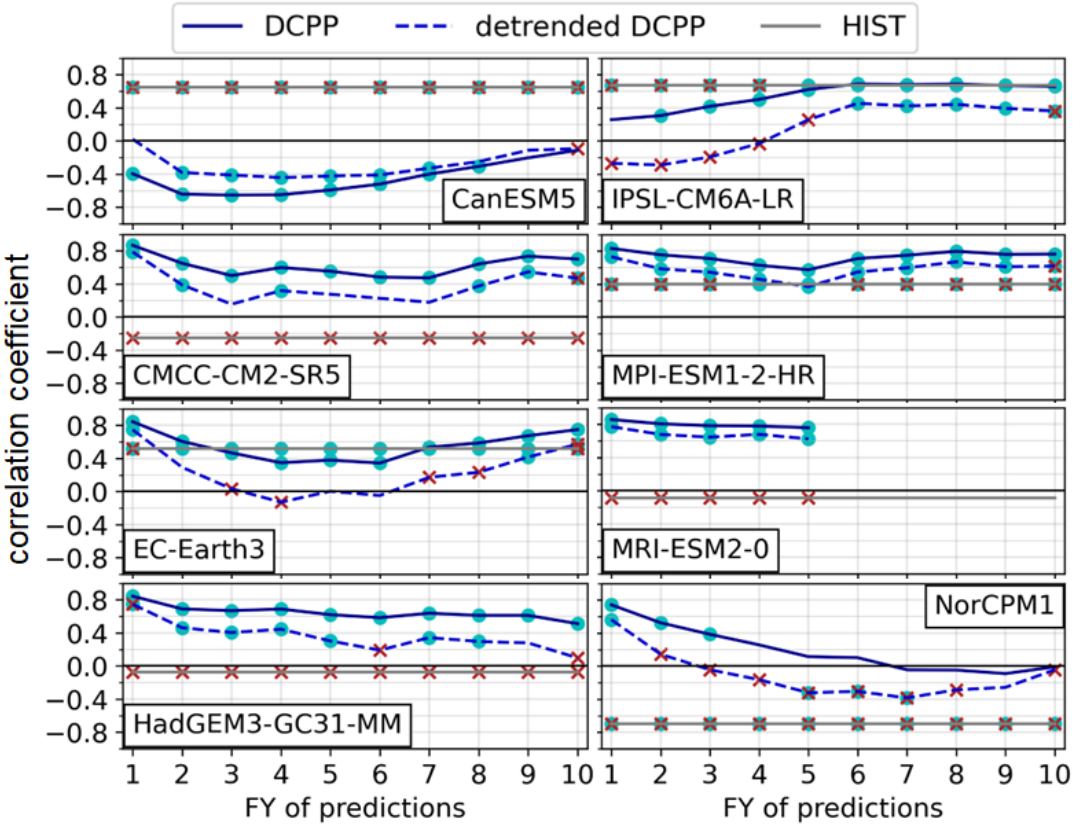

Figure 5. ACC of the spatially averaged OHC700 in the Labrador Sea (red box in Figure 2) as a function of FY. Skill values are shown for the DCPP (blue lines) and HIST ensembles (grey lines) and are evaluated against EN4. In DCPP, skill is also computed after detrending both the forecast anomalies and the EN4 anomalies (detrended DCPP; dashed blue lines). Cyan dots indicate ACC values that are significantly different from zero at the 95% confidence level. Red crosses indicate that the HIST or the detrended DCPP ACC values are significantly different from the DCPP values.

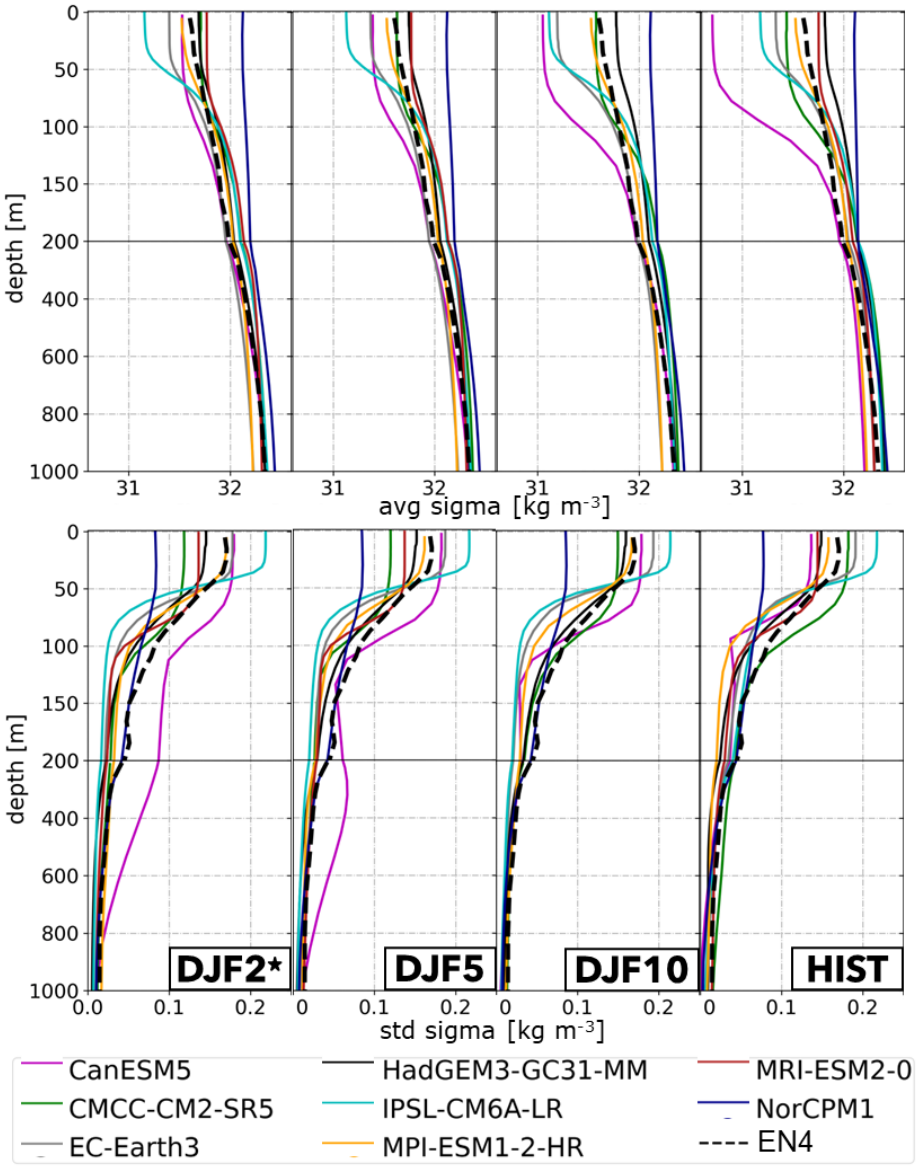

Figure 6. (Top) Mean-state climatology of the spatially averaged LS potential density anomaly in DJF (referred to 1000 m; *sigma1*) as a function of depth. The observational reference EN4 is included as a dashed black line. From left to right, it shows the results for the DCPP (in forecast winters DJF2, DJF5 and DJF10) and HIST (in DJF) ensembles over the period 1970-2014. (Bottom) The same as in the top row, but for the standard deviation in time of the spatially averaged LS potential density anomaly.

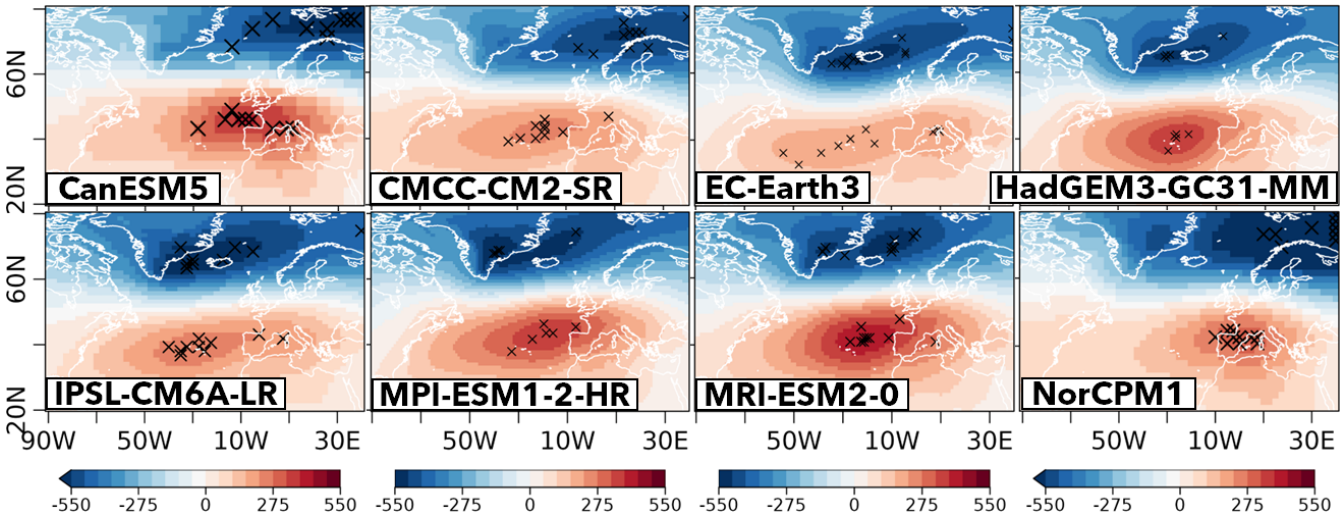

Figure 7. Spatial patterns of the NAO (as described by the first EOF of DJF sea level pressure) in the different HIST ensembles. The EOF is computed with all individual model members concatenated in time. Each cross represents the positive and negative centres of action (defined at the place where the NAO pattern attains its maximum and minimum sea level pressure anomalies) when the EOF is computed individually for each member, to thus indicate the intra-model spread.

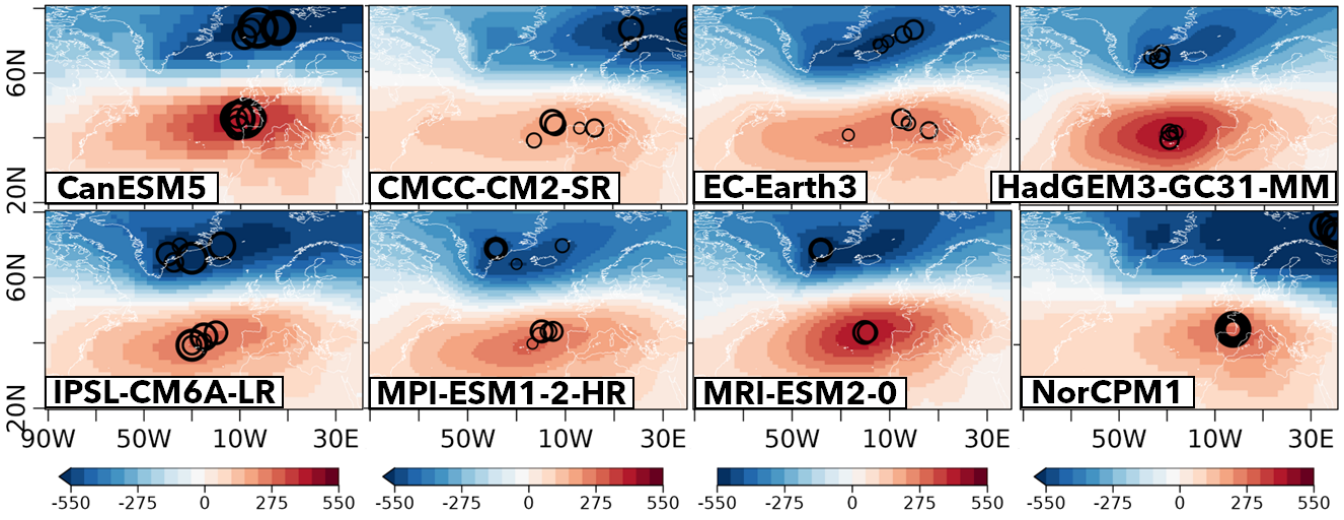

Figure 8. Same as in Figure 7 but for DCPP experiments. In this case the colour shading represents the NAO pattern at DJF2 and the circles (in increasing size) represent the centres of action of the ensemble mean for DJF2, 4, 6, 8 and 10, to thus illustrate any potential shifts with forecast time.

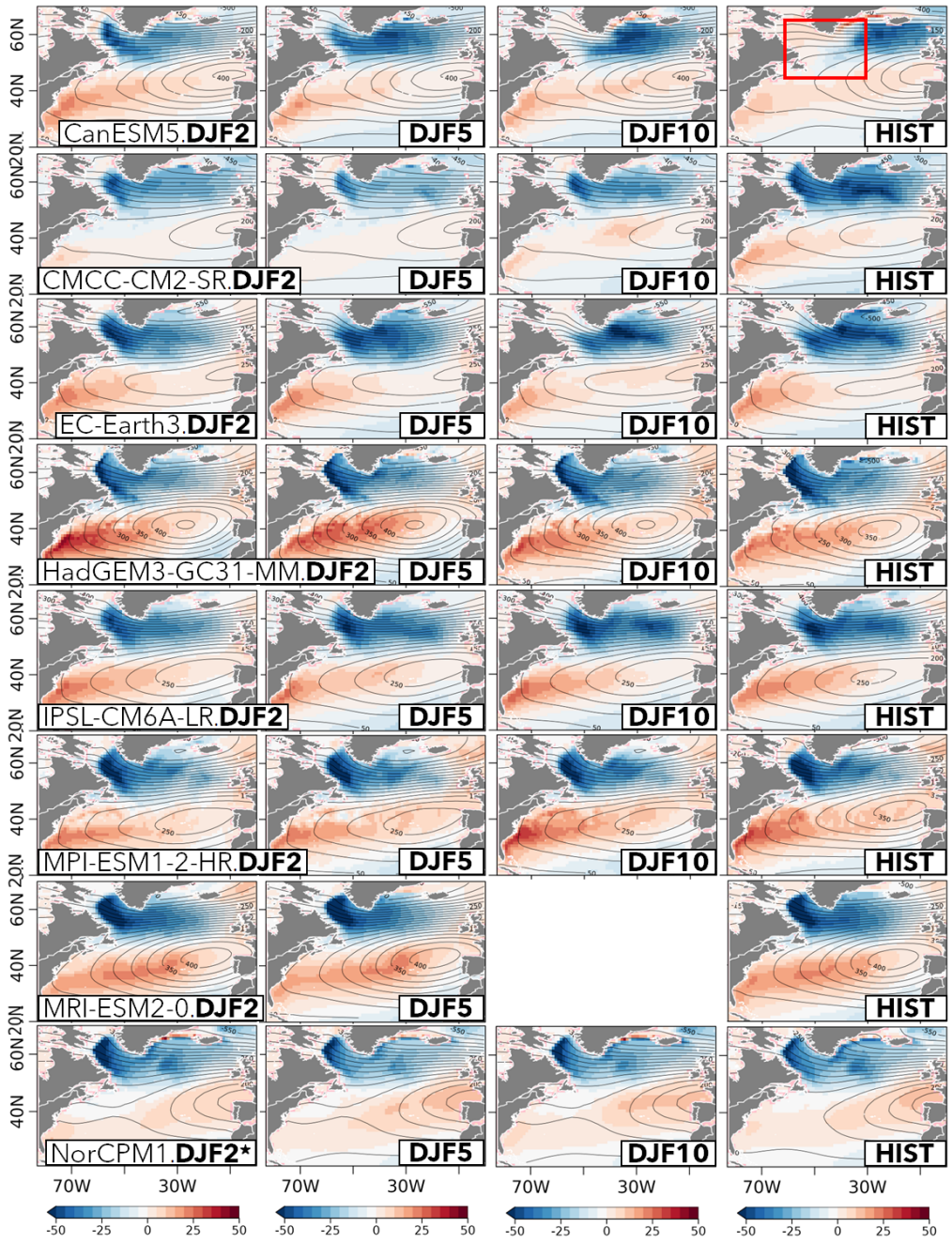

Figure 9. Regression maps of the NAO index onto net surface heat fluxes (*hfds*) for the DCPP (in forecast winters DJF2, DJF5 and DJF10; columns 1-3, respectively) and HIST ensembles (in DJF; column 4). Negative (positive) values represent upward (downward) heat fluxes, in Wm^{-2}. The contour lines represent the corresponding NAO pattern. The red box in the upper-right plot depicts the LS region used in the analyses.

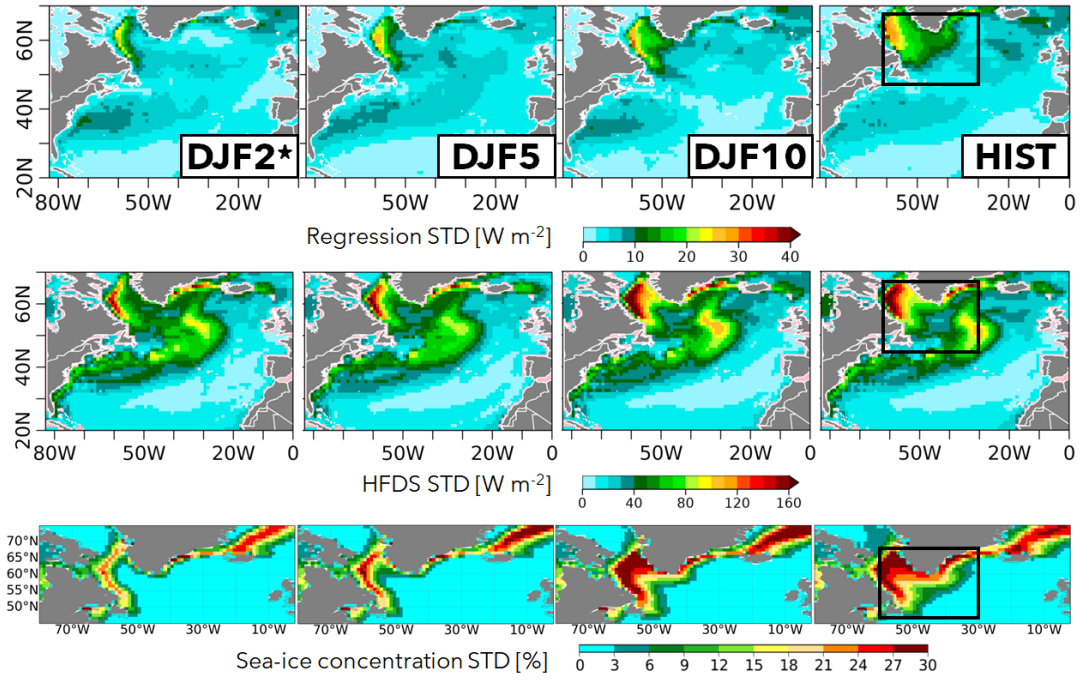

Figure 10. (Top) Inter-model spread for the regression coefficients in Figure 9, as defined by the standard deviation across models. (Middle) The same as above but for the climatological net surface heat fluxes in DJF. (Bottom) The same as above but for the climatological sea ice concentration in DJF. The black box in the rightmost column depicts the LS region used in the analyses.

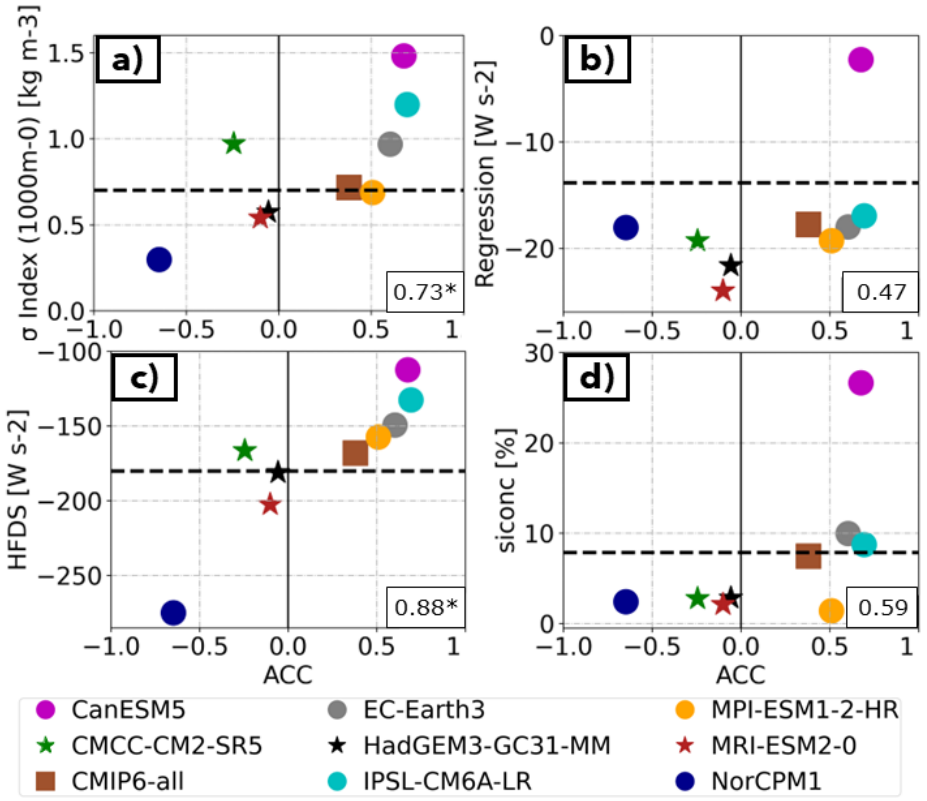

Figure 11. (a) Scatterplot of the relationship between the ACC skill in the Labrador Sea OHC700 and the climatological value of index of the Labrador Sea density stratification in the HIST ensembles. The stratification index is computed as the density difference between 1000m and the surface. The 1000m level was chosen based on the visual inspection of the vertical profiles (Figure 6) as a characteristic level of the mean properties of the ocean subsurface. Larger values of the index correspond to models where the LS is more stratified. (b) The same as in *a* but between the ACC skill in the Labrador Sea OHC700 and the regressed values of the NAO index onto the Labrador Sea net surface heat fluxes in DJF. (c) The same as in *a* but between the ACC skill in the Labrador Sea OHC700 and the climatological Labrador Sea net surface heat fluxes in DJF; d) The same as in *a* but between the ACC skill in the Labrador Sea OHC700 and climatological DJF sea-ice concentrations in the Labrador Sea. In all panels stars represent non-significant correlation values at the 95% confidence level. The black dashed horizontal line represents the respective reference dataset: a) EN4; b,c) ERA5; d) HadISST. The linear relationship between the different pairs of metrics is measured with correlation values in the model space, shown for each plot in the lower right corners, with asterisks indicating if the correlation coefficient is significant at the 95% confidence level.

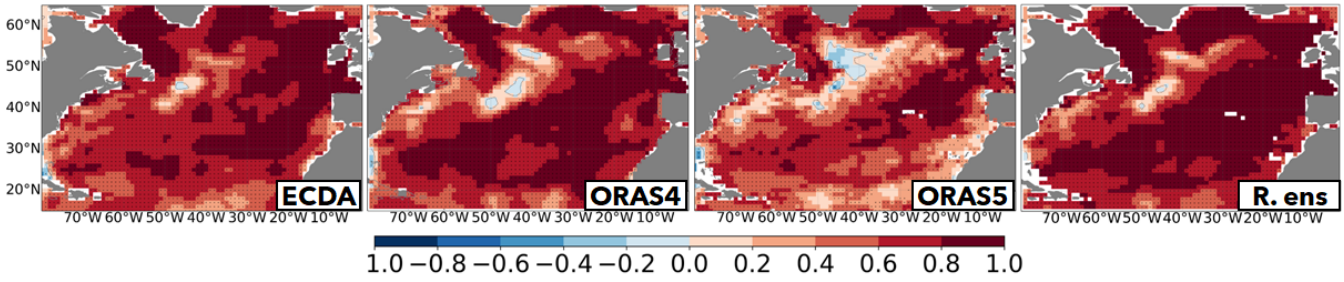

Figure A1. Correlation maps between the OHC700 in EN4 and the OHC700 in ECDA, ORAS4, ORAS5 and the multi-reanalyses ensemble mean, computed over the period 1970-2014.

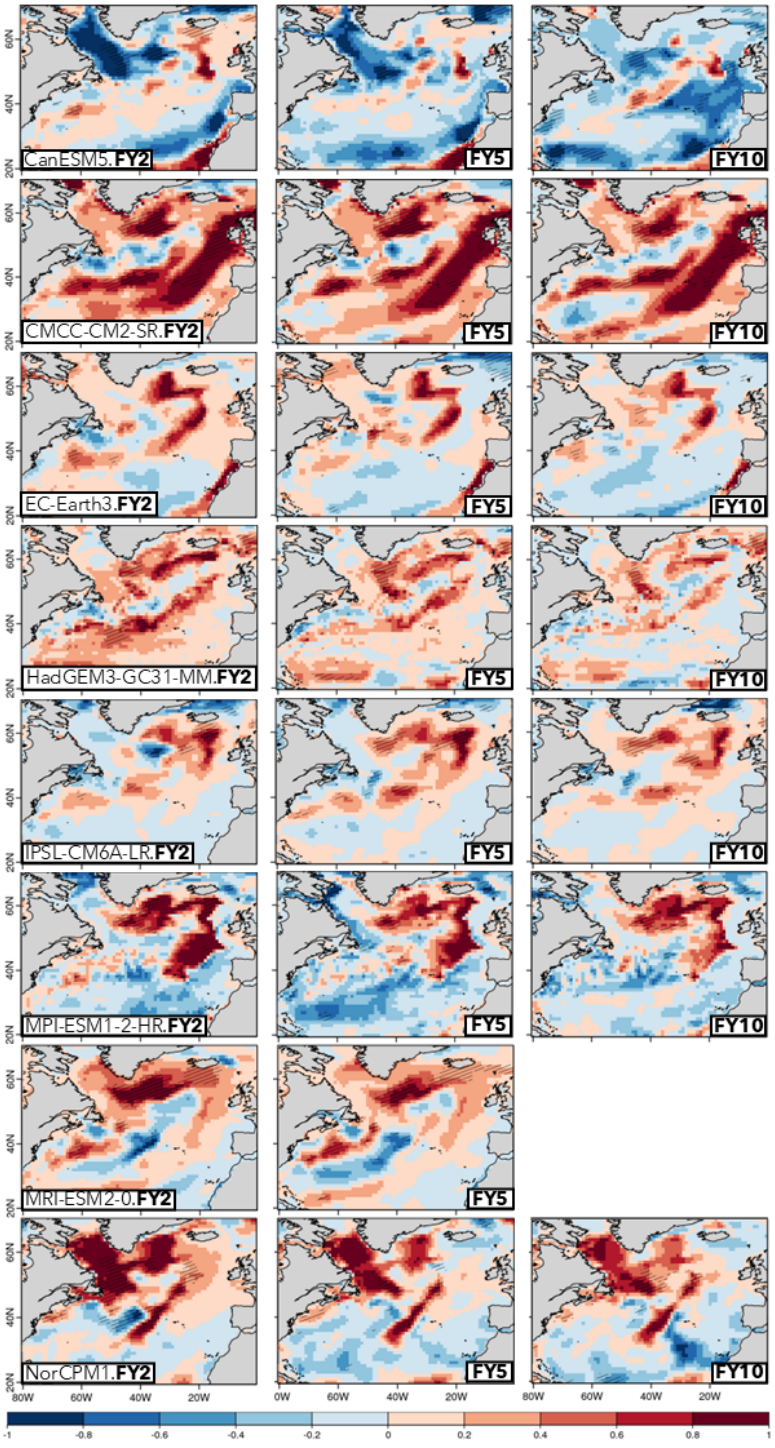

Figure A2. The same as in Figure 1 but for the difference in ACC values between the DCPP and HIST ensembles.

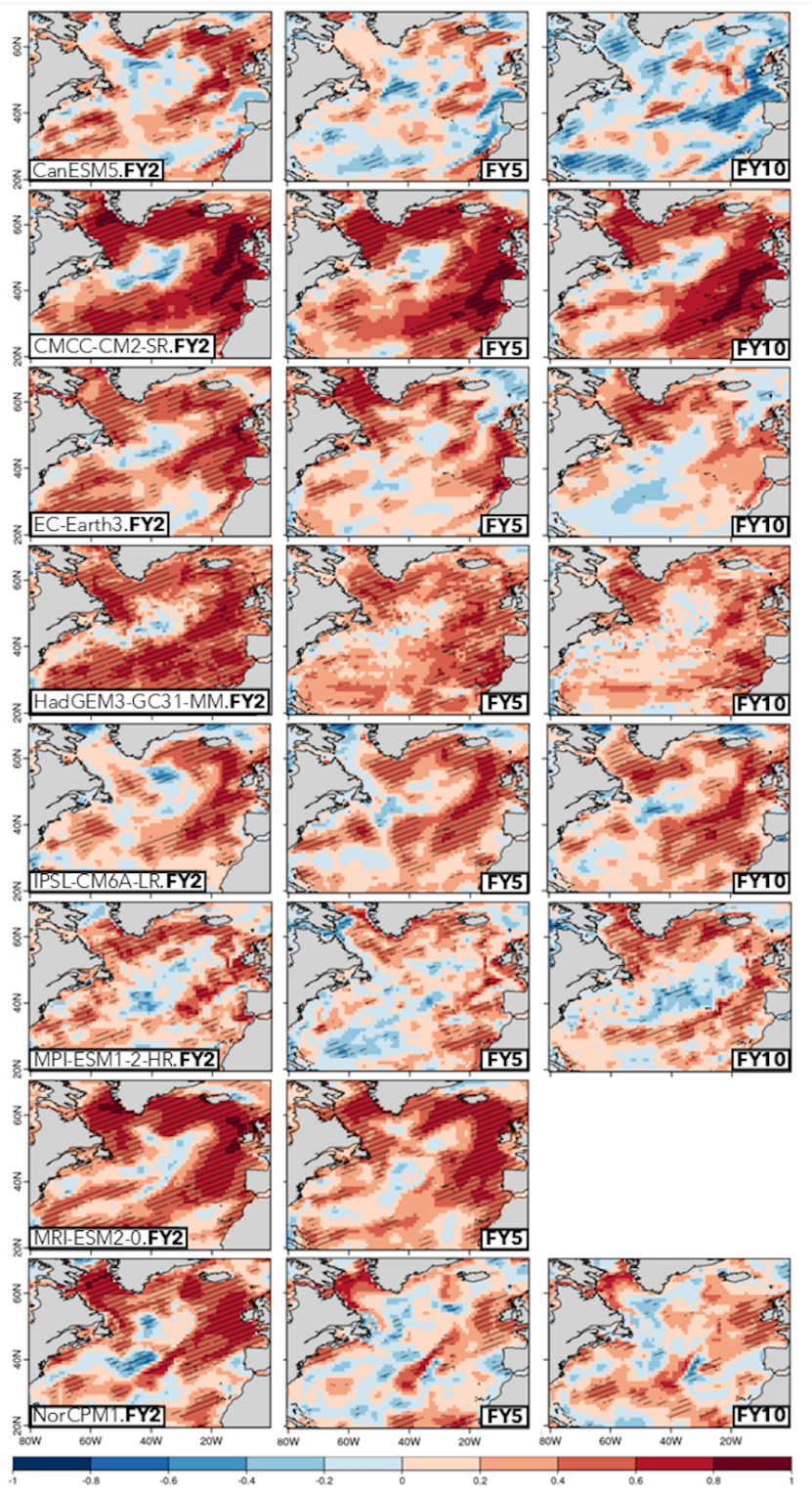

Figure A3. The same as in Figure 1 but for the residual correlations in each DCPP ensemble.

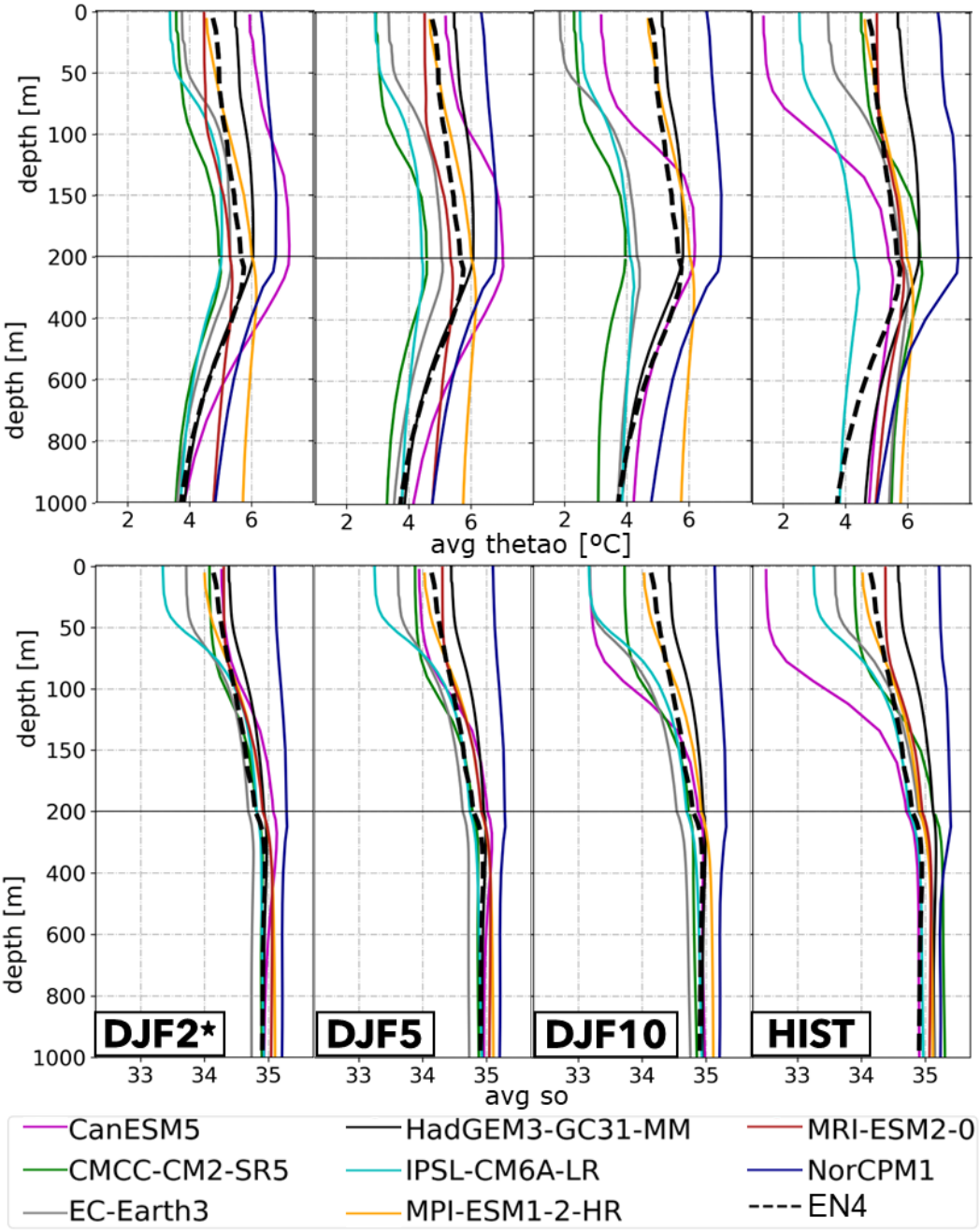

Figure A4. As in Figure 6 but for the climatological vertical profiles of potential temperature (top) and salinity (bottom).

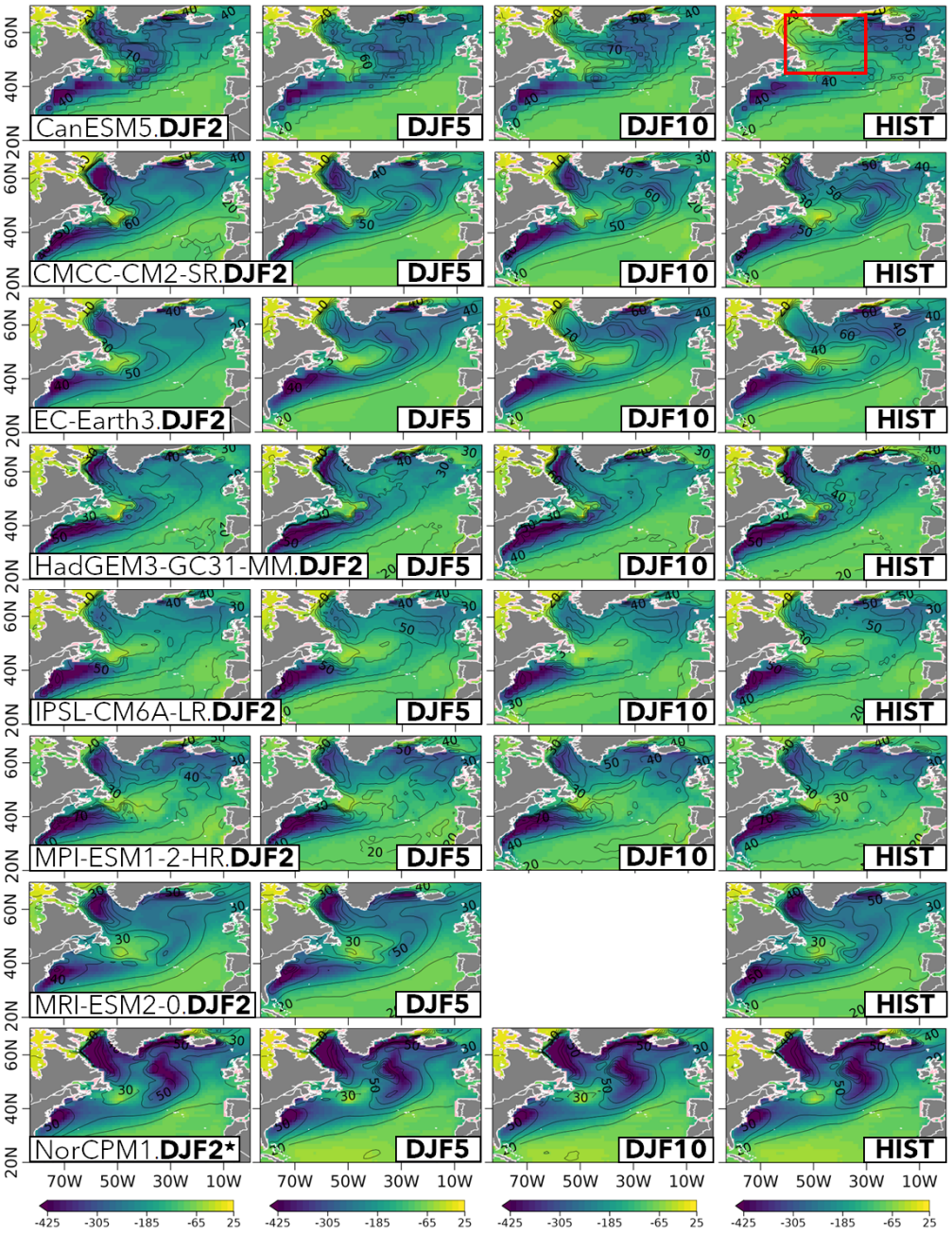

Figure A5. Climatological DJF net surface heat fluxes for the DCPP (in forecast winters DJF2, DJF5 and DJF10; columns 1-3, respectively) and HIST ensembles (in DJF, column 4). Negative (positive) values represent upward (downward) heat fluxes, in Wm^{-2}. The contour lines represent the associated standard deviation in time for the period 1970-2014. The red box in the upper-right plot depicts the LS region used in the analyses.

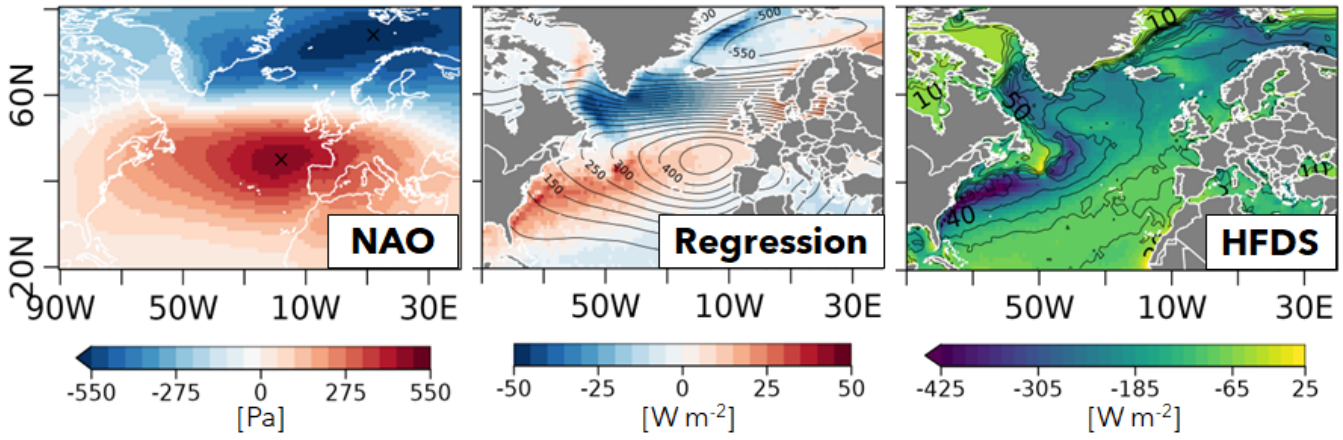

Figure A6. (Left) Spatial pattern of the NAO in the ERA5 reanalysis, computed as in Figure 7. (Middle) Regression map of the NAO index onto the DJF net surface heat fluxes in the ERA5 reanalysis. (Right) Climatological DJF net surface fluxes in the ERA5 reanalyses.

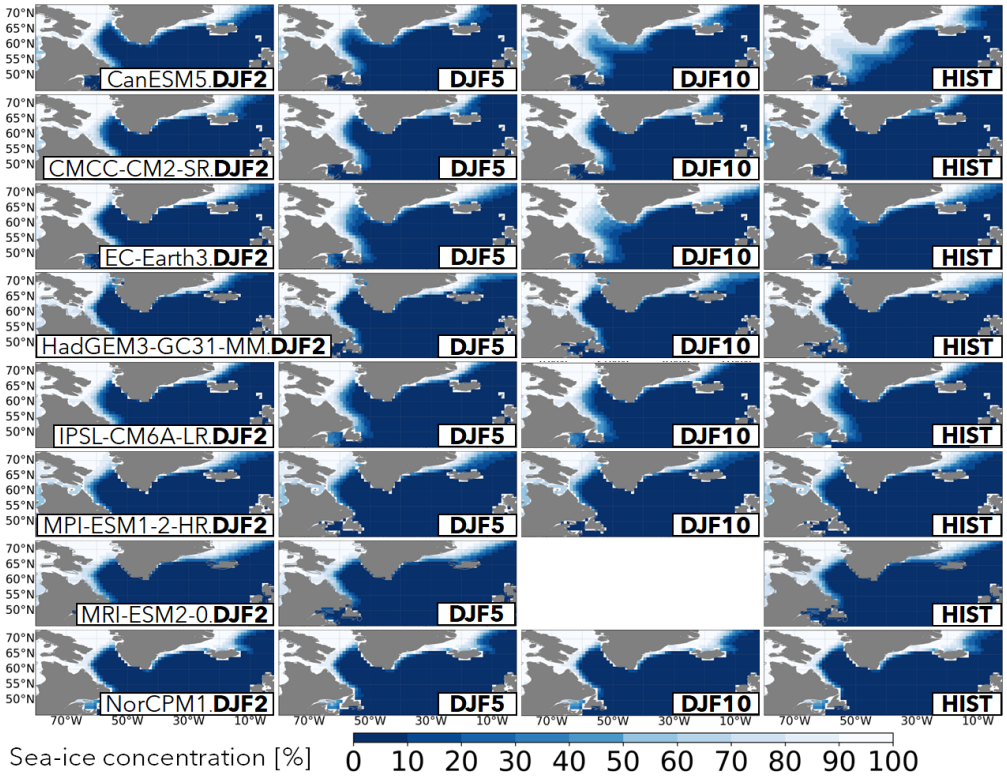

Figure A7. Sea ice concentration (*siconc*) maps for the initialized predictions for the forecast winters DJF2, DJF5 and DJF10 (columns 1-3, respectively) as well as DJF in the HIST ensemble (column 4).

Author contributions. TCC wrote the original draft with input from all authors, specially RB and PO. TCC wrote the scripts to analyse the data and to plot the figures. All authors contributed to the conceptualization of the study and to the interpretation of the results.

Competing interests. The authors have no conflicts of interest to declare that are relevant to the content of this article.

Acknowledgements. TCC would like to acknowledge the financial support from the the FCT (Fundação para a Ciência e a Tecnologia) through projects FCT-UIDB/50019/2020, PD/BD/142785/2018 and COVID/BD/152668/2022. Furthermore, ATM acknowledges SARDINHA2020 (MAR2020) and ROADMAP (JPIOCEANS/ 0001/2019). RB was supported by the European Commission H2020 projects EUCP (Grant no. 776613) and the Horizon Europe Project Impetus4Change (Grant no. 101081555). PO was supported by the Spanish Ministry of Economy, Industry and Competitiveness through the Ramon y Cajal grant RYC-2017-22772. JR was funded by NERC via the WISHBONE (NE/T013516/1), CANARI (NE/W004984/1), and ALPACA (NE/W004984/1) projects, and by UKRI via the EPOC project.

References

Athanasiadis, P. J., Yeager, S., Kwon, Y.-O., Bellucci, A., Smith, D. W., and Tibaldi, S.: Decadal predictability of North Atlantic blocking and the NAO, npj Climate and Atmospheric Science, 3, 20, https://doi.org/10.1038/s41612-020-0120-6, 2020.

Balaguru, K., Foltz, G. R., and Leung, L. R.: Increasing Magnitude of Hurricane Rapid Intensification in the Central and Eastern Tropical Atlantic, Geophysical Research Letters, 45, 4238–4247, https://doi.org/10.1029/2018GL077597, 2018.

Balmaseda, M. A., Mogensen, K., and Weaver, A. T.: Evaluation of the ECMWF ocean reanalysis system ORAS4, Quarterly Journal of the Royal Meteorological Society, 139, 1132–1161, https://doi.org/10.1002/qj.2063, 2013.

Bethke, I., Wang, Y., Counillon, F., Keenlyside, N., Kimmritz, M., Fransner, F., Samuelsen, A., Langehaug, H., Svendsen, L., Chiu, P. G., Passos, L., Bentsen, M., Guo, C., Gupta, A., Tjiputra, J., Kirkeväg, A., Olivié, D., Seland, Ø., Solsvik Vägane, J., Fan, Y., and Eldevik, T.: NorCPM1 and its contribution to CMIP6 DCPP, Geoscientific Model Development, 14, 7073–7116, https://doi.org/10.5194/gmd-14-7073-2021, 2021.

Bilbao, R., Wild, S., Ortega, P., Acosta-Navarro, J., Arsouze, T., Bretonnière, P. A., Caron, L. P., Castrillo, M., Cruz-García, R., Cvijanovic, I., Javier Doblas-Reyes, F., Donat, M., Dutra, E., Echevarría, P., Ho, A. C., Loosveldt-Tomas, S., Moreno-Chamarro, E., Pérez-Zanon, N., Ramos, A., Ruprich-Robert, Y., Sicardi, V., Tourigny, E., and Vegas-Regidor, J.: Assessment of a full-field initialized decadal climate prediction system with the CMIP6 version of EC-Earth, Earth System Dynamics, 12, 173–196, https://doi.org/10.5194/esd-12-173-2021, 2021.

Bilbao, R. A. F., Gregory, J. M., Bouttes, N., Palmer, M. D., and Stott, P.: Attribution of ocean temperature change to anthropogenic and natural forcings using the temporal, vertical and geographical structure, Climate Dynamics, 53, 5389–5413, https://doi.org/10.1007/s00382-019-04910-1, 2019.

Boer, G. J., Smith, D. M., Cassou, C., Doblas-Reyes, F., Danabasoglu, G., Kirtman, B., Kushnir, Y., Kimoto, M., Meehl, G. A., Msadek, R., Mueller, W. A., Taylor, K. E., Zwiers, F., Rixen, M., Ruprich-Robert, Y., and Eade, R.: The Decadal Climate Prediction Project (DCPP) contribution to CMIP6, Geoscientific Model Development, 9, 3751–3777, https://doi.org/10.5194/gmd-9-3751-2016, 2016.

Bonnet, R., Boucher, O., Deshayes, J., Gastineau, G., Hourdin, F., Mignot, J., Servonnat, J., and Swingedouw, D.: Presentation and Evaluation of the IPSL-CM6A-LR Ensemble of Extended Historical Simulations, Journal of Advances in Modeling Earth Systems, 13, https://doi.org/10.1029/2021MS002565, 2021.

Borchert, L. F., Müller, W. A., and Baehr, J.: Atlantic ocean heat transport influences interannual-to-decadal surface temperature predictability in the North Atlantic Region, Journal of Climate, 31, 6763–6782, https://doi.org/10.1175/JCLI-D-17-0734.1, 2018.

Buckley, M. W. and Marshall, J.: Observations, inferences, and mechanisms of the Atlantic Meridional Overturning Circulation: A review, Reviews of Geophysics, 54, 5–63, https://doi.org/10.1002/2015RG000493, 2016.

Buckley, M. W., DelSole, T., Lozier, M. S., and Li, L.: Predictability of North Atlantic Sea surface temperature and upper-ocean heat content, Journal of Climate, 32, 3005–3023, https://doi.org/10.1175/JCLI-D-18-0509.1, 2019.

Caesar, L., McCarthy, G. D., Thornalley, D. J., Cahill, N., and Rahmstorf, S.: Current Atlantic Meridional Overturning Circulation weakest in last millennium, Nature Geoscience, 14, 118–120, https://doi.org/10.1038/s41561-021-00699-z, 2021.

Carmo-Costa, T., Bilbao, R., Ortega, P., Teles-Machado, A., and Dutra, E.: Trends, variability and predictive skill of the ocean heat content in North Atlantic: an analysis with the EC-Earth3 model, Climate Dynamics, 58, 1311–1328 (2022), https://doi.org/10.1007/s00382-021-05962-y, 2021.

Chang, Y. S., Zhang, S., Rosati, A., Delworth, T. L., and Stern, W. F.: An assessment of oceanic variability for 1960-2010 from the GFDL ensemble coupled data assimilation, Climate Dynamics, 40, 775–803, https://doi.org/10.1007/s00382-012-1412-2, 2013.

Cherchi, A., Fogli, P. G., Lovato, T., Peano, D., Iovino, D., Gualdi, S., Masina, S., Scoccimarro, E., Materia, S., Bellucci, A., and Navarra, A.: Global Mean Climate and Main Patterns of Variability in the CMCC-CM2 Coupled Model, Journal of Advances in Modeling Earth Systems, 11, 185–209, https://doi.org/10.1029/2018MS001369, 2019.

Delgado-Torres, C., Donat, M. G., Gonzalez-Reviriego, N., Caron, L.-P., Athanasiadis, P. J., Bretonnière, P.-A., Dunstone, N. J., Ho, A.-C., Nicoli, D., Pankatz, K., Paxian, A., Pérez-Zanón, N., Cabré, M. S., Solaraju-Murali, B., Soret, A., and Doblas-Reyes, F. J.: Multi-Model Forecast Quality Assessment of CMIP6 Decadal Predictions, Journal of Climate, 35, 4363–4382, https://doi.org/10.1175/JCLI-D-21-0811.1, 2022.

Doblas-Reyes, F. J., Andreu-Burillo, I., Chikamoto, Y., García-Serrano, J., Guemas, V., Kimoto, M., Mochizuki, T., Rodrigues, L. R. L., and van Oldenborgh, G. J.: Initialized near-term regional climate change prediction, Nature Communications, 4, 1–9, https://doi.org/10.1038/ncomms2704, 2013.

Döscher, R., Acosta, M., Alessandri, A., Anthoni, P., Arneth, A., Arsouze, T., Bergman, T., Bernardello, R., Bousetta, S., Caron, L.-P., Carver, G., Castrillo, M., Catalano, F., Cvijanovic, I., Davini, P., Dekker, E., Doblas-Reyes, F. J., Docquier, D., Echevarria, P., Fladrich, U., Fuentes-Franco, R., Gröger, M., Hardenberg, J. V., Hieronymus, J., Karami, M. P., Keskinen, J.-P., Koenigk, T., Makkonen, R., Massonnet, F., Ménégoz, M., Miller, P. A., Moreno-Chamarro, E., Nieradzik, L., van Noije, T., Nolan, P., O'donnell, D., Ollinaho, P. P., van den Oord, G., Ortega, P., Prims, O. T., Ramos, A., Reerink, T., Rousset, C., Ruprich-Robert, Y., Le Sager, P., Schmith, T., Schrödner, R., Serva, F., Sicardi, V., Madsen, M. S., Smith, B., Tian, T., Tourigny, E., Uotila, P., Vancoppenolle, M., Wang, S., Wårlind, D., Willén, U., Wyser, K., Yang, S., Yepes-Arbós, X., Zhang, Q., Bergmann, T., Bernadello, R., Bousetta, S., Caron, L.-P., Carver, G., Castrillo, M., Catalano, F., Cvijanovic, I., Davini, P., Dekker, E., Doblas-Reyes, F. J., Docquier, D., Echevarria, P., Fladrich, U., Fuentes-Franco, R., Gröger, M., v. Hardenberg, J., Hieronymus, J., Karami, M. P., Keskinen, J.-P., Koenigk, T., Makkonen, R., Massonnet, F., Ménégoz, M., Miller, P. A., Moreno-Chamarro, E., Nieradzik, L., van Noije, T., Nolan, P., O'Donnell, D., Ollinaho, P. P., van den Oord, G., Ortega, P., Prims, O. T., Ramos, A., Reerink, T., Rousset, C., Ruprich-Robert, Y., Le Sager, P., Schmith, T., Schrödner, R., Serva, F., Sicardi, V., Sloth Madsen, M., Smith, B., Tian, T., Tourigny, E., Uotila, P., Vancoppenolle, M., Wang, S., Wårlind, D., Willén, U., Wyser, K., Yang, S., Yepes-Arbós, X., and Zhang, Q.: The EC-Earth3 Earth System Model for the Climate Model Intercomparison Project 6, Geoscientific Model Development Discussions, pp. 1–90, https://doi.org/10.5194/gmd-2020-446, 2021.

Drijfhout, S., van Oldenborgh, G. J., and Cimatoribus, A.: Is a decline of AMOC causing the warming hole above the North Atlantic in observed and modeled warming patterns?, Journal of Climate, 25, 8373–8379, https://doi.org/10.1175/JCLI-D-12-00490.1, 2012.

Durack, P. J., Gleckler, P. J., Purkey, S. G., Johnson, G. C., Lyman, J. M., and Boyer, T. P.: Ocean Warming: From the Surface to the Deep in Observations and Models, Oceanography, 31, 10.5670/oceanog.2018.227, 2018.

Eden, C. and Jung, T.: North Atlantic interdecadal variability: Oceanic response to the North Atlantic oscillation (1865-1997), Journal of Climate, 14, 676–691, https://doi.org/10.1175/1520-0442(2001)014<0676:NAIVOR>2.0.CO;2, 2001.

Enfield, D. B., Mestas-Nunez, A. M., and Trimble, P. J.: The Atlantic Multidecadal Oscillation and its relation to rainfall and river flows in the continental U.S., Geophysical Research Letters, 28, 2077–2080, https://doi.org/10.1029/2000GL012745, 2001.

Eyring, V., Bony, S., Meehl, G. A., Senior, C. A., Stevens, B., Stouffer, R. J., and Taylor, K. E.: Overview of the Coupled Model Intercomparison Project Phase 6 (CMIP6) experimental design and organization., Geoscientific Model Development, European Geosciences Union, 9, 1937–1958, https://doi.org/10.5194/gmd-9-1937-2016, 2016.

Gastineau, G. and Frankignoul, C.: Influence of the North Atlantic SST Variability on the Atmospheric Circulation during the Twentieth Century, Journal of Climate, 28, 1396 – 1416, https://doi.org/10.1175/JCLI-D-14-00424.1, 2015.

Gleckler, P. J., Santer, B. D., Domingues, C. M., Pierce, D. W., Barnett, T. P., Church, J. A., Taylor, K. E., AchutaRao, K. M., Boyer, T. P., Ishii, M., and Caldwell, P. M.: Human-induced global ocean warming on multidecadal timescales, Nature Climate Change, 2, 524–529, https://doi.org/10.1038/nclimate1553, 2012.

Good, S. A., Martin, M. J., and Rayner, N. A.: EN4: Quality controlled ocean temperature and salinity profiles and monthly objective analyses with uncertainty estimates, Journal of Geophysical Research: Oceans, 118, 6704–6716, https://doi.org/10.1002/2013JC009067, 2013.

Gouretski, V. and Reseghetti, F.: On depth and temperature biases in bathythermograph data: Development of a new correction scheme based on analysis of a global ocean database, Deep Sea Research Part I: Oceanographic Research Papers, 57, 812–833, https://doi.org/10.1016/j.dsr.2010.03.011, 2010.

Guemas, V. and Salas, M. D.: Simulation of the Atlantic meridional overturning circulation in an atmosphere-ocean global coupled model. Part I: A mechanism governing the variability of ocean convection in a preindustrial experiment, Climate Dynamics, 31, 29–48, https://doi.org/10.1007/s00382-007-0336-8, 2008.

Guemas, V., Manubens, N., Garcia-Serrano, J., Fuckar, N., Caron, L.-P., Bellprat, O., Rodrigues, L., Torralba, V., Hunter, A., Prodhomme, C., Menegoz, M., Manubens, D., Ardilouze, C., Batte, L., Lienert, F., Giner, J., Baudouin, J.-P., Gonzalez, N., Auger, L., Cortesi, N., Exarchou, E., Cruz, R., Andreu-Burillo, I., Saurral, R., Manubens, D., Lienert, F., Garcia-Serrano, J., Batte, L., Caron, L.-P., Rodrigues, L., Menegoz, M., Fuckar, N., Manubens, N., Bellprat, O., Torralba, V., and Guemas, V.: Package 's2dverification' : Set of Common Tools for Forecast Verification, Tech. rep., BSC, Barcelona, 2019.

Häkkinen, S., Rhines, P. B., and Worthen, D. L.: Heat content variability in the North Atlantic Ocean in ocean reanalyses, Geophysical Research Letters, 42, 2901–2909, https://doi.org/10.1002/2015GL063299, 2015.

Hazeleger, W., Guemas, V., Wouters, B., Corti, S., Andreu-Burillo, I., Doblas-Reyes, F. J., Wyser, K., and Caian, M.: Multiyear climate predictions using two initialization strategies, Geophysical Research Letters, 40, 1794–1798, https://doi.org/10.1002/grl.50355, 2013.

Hegerl, G. C., Ballinger, A. P., Booth, B. B. B., Borchert, L. F., Brunner, L., Donat, M. G., Doblas-Reyes, F. J., Harris, G. R., Lowe, J., Mahmood, R., Mignot, J., Murphy, J. M., Swingedouw, D., and Weisheimer, A.: Toward Consistent Observational Constraints in Climate Predictions and Projections, Frontiers in Climate, 3, https://doi.org/10.3389/fclim.2021.678109, 2021.

Hermanson, L., Eade, R., Robinson, N. H., Dunstone, N. J., Andrews, M. B., Knight, J. R., Scaife, A. A., and Smith, D. M.: Forecast cooling of the Atlantic subpolar gyre and associated impacts, Geophysical Research Letters, 41, 5167–5174, https://doi.org/10.1002/2014GL060420, 2014.

Hersbach, H., Bell, B., Berrisford, P., Hirahara, S., Horányi, A., Muñoz-Sabater, J., Nicolas, J., Peubey, C., Radu, R., Schepers, D., Simmons, A., Soci, C., Abdalla, S., Abellan, X., Balsamo, G., Bechtold, P., Biavati, G., Bidlot, J., Bonavita, M., De Chiara, G., Dahlgren, P., Dee, D., Diamantakis, M., Dragani, R., Flemming, J., Forbes, R., Fuentes, M., Geer, A., Haimberger, L., Healy, S., Hogan, R. J., Hólm, E., Janisková, M., Keeley, S., Laloyaux, P., Lopez, P., Lupu, C., Radnoti, G., de Rosnay, P., Rozum, I., Vamborg, F., Villaume, S., and Thépaut, J. N.: The ERA5 global reanalysis, Quarterly Journal of the Royal Meteorological Society, 146, 1999–2049, https://doi.org/10.1002/qj.3803, 2020.

Hurrell, J. W.: Decadal Trends in the North Atlantic Oscillation: Regional Temperatures and Precipitation, Science, 269, 7–10, https://doi.org/10.1126/science.269.5224.676, 1995.

IPCC: Climate Change 2021: The Physical Science Basis. Contribution of Working Group I to the Sixth Assessment Report of the Intergovernmental Panel on Climate Change, vol. In Press, Cambridge University Press, Cambridge, United Kingdom and New York, NY, USA, https://doi.org/10.1017/9781009157896, 2021.

Johnson, G. C. and Lyman, J. M.: Warming trends increasingly dominate global ocean, Nature Climate Change, 10, 757–761, https://doi.org/10.1038/s41558-020-0822-0, 2020.

Josey, S. A., Hirschi, J. J.-M., Sinha, B., Duchez, A., Grist, J. P., and Robert Marsh: The Recent Atlantic Cold Anomaly: Causes, Consequences, and Related Phenomena, Annual Review of Marine Science, 10, 475–501, https://doi.org/10.1146/annurev-marine-121916, 2018.

Kay, G., Dunstone, N. J., Smith, D. M., Betts, R. A., Cunningham, C., and Scaife, A. A.: Assessing the chance of unprecedented dry conditions over North Brazil during El Niño events, Environmental Research Letters, 17, https://doi.org/10.1088/1748-9326/ac6df9, 2022.

Keenlyside, N. S., Latif, M., Jungclaus, J., Kornblueh, L., and Roeckner, E.: Advancing decadal-scale climate prediction in the North Atlantic sector, Nature, 453, 84–88, https://doi.org/10.1038/nature06921, 2008.

Keil, P., Mauritsen, T., Jungclaus, J., Hedemann, C., Olonscheck, D., and Ghosh, R.: Multiple drivers of the North Atlantic warming hole, Nature Climate Change 2020 10:7, 10, 667–671, https://doi.org/10.1038/s41558-020-0819-8, 2020.

Kim, H.-J., An, S.-I., Park, J.-H., Sung, M.-K., Kim, D., Choi, Y., and Kim, J.-S.: North Atlantic Oscillation impact on the Atlantic Meridional Overturning Circulation shaped by the mean state, npj Climate and Atmospheric Science, 6, 25, 2023a.

Kim, W. M., Yeager, S. G., Danabasoglu, G., and Chang, P.: Exceptional multi-year prediction skill of the Kuroshio Extension in the CESM high-resolution decadal prediction system, npj Climate and Atmospheric Science, 6, 118, https://doi.org/10.1038/s41612-023-00444-w, 2023b.

Knight, J. R., Allan, R. J., Folland, C. K., Vellinga, M., and Mann, M. E.: A signature of persistent natural thermohaline circulation cycles in observed climate, Geophysical Research Letters, 32, 1–4, https://doi.org/10.1029/2005GL024233, 2005.

Kröger, J., Pohlmann, H., Sienz, F., Marotzke, J., Baehr, J., Köhl, A., Modali, K., Polkova, I., Stammer, D., Vamborg, F. S., and Müller, W. A.: Full-field initialized decadal predictions with the MPI earth system model: an initial shock in the North Atlantic, Climate Dynamics, 51, 2593–2608, https://doi.org/10.1007/s00382-017-4030-1, 2018.

Kwon, Y. O., Seo, H., Ummenhofer, C. C., and Joyce, T. M.: Impact of multidecadal variability in Atlantic SST on winter atmospheric blocking, Journal of Climate, 33, 867–892, https://doi.org/10.1175/JCLI-D-19-0324.1, 2020.

Langehaug, H. R., Ortega, P., Counillon, F., Matei, D., Maroon, E., Keenlyside, N., Mignot, J., Wang, Y., Swingedouw, D., Bethke, I., Yang, S., Danabasoglu, G., Bellucci, A., Ruggieri, P., Nicoli, D., and Orthun, M.: Propagation of Thermohaline Anomalies and Their Predictive Potential along the Atlantic Water Pathway, Journal of Climate, 35, 2111 – 2131, https://doi.org/10.1175/JCLI-D-20-1007.1, 2022.

Levitus, S., Antonov, J. I., Boyer, T. P., and Stephens, C.: Warming of the World Ocean, Science, 287, 2225–2229, https://doi.org/10.1126/science.287.5461.2225, 2000.

Levitus, S., Antonov, J. I., Boyer, T. P., Baranova, O. K., Garcia, H. E., Locarnini, R. A., Mishonov, A. V., Reagan, J. R., Seidov, D., Yarosh, E. S., and Zweng, M. M.: World ocean heat content and thermosteric sea level change (0-2000m), 1955-2010, Geophysical Research Letters, 39, 1–5, https://doi.org/10.1029/2012GL051106, 2012.

Li, H., Ilyina, T., Müller, W. A., and Landschützer, P.: Predicting the variable ocean carbon sink, Science Advances, 5, 1–9, https://doi.org/10.1126/sciadv.aav6471, 2019.

Manubens, N., Caron, L. P., Hunter, A., Bellprat, O., Exarchou, E., Fučkar, N. S., Garcia-Serrano, J., Massonnet, F., Ménégoz, M., Sicardi, V., Batté, L., Prodhomme, C., Torralba, V., Cortesi, N., Mula-Valls, O., Serradell, K., Guemas, V., and Doblas-Reyes, F. J.: An R package for climate forecast verification, Environmental Modelling and Software, 103, 29–42, https://doi.org/10.1016/j.envsoft.2018.01.018, 2018.

Maroon, E. A., Yeager, S. G., Danabasoglu, G., and Rosenbloom, N.: Was the 2015 North Atlantic Subpolar Cold Anomaly Predictable?, Journal of Climate, 34, 5403 – 5423, https://doi.org/10.1175/JCLI-D-20-0750.1, 2021.

Mecking, J. V., Drijfhout, S. S., Hirschi, J. J., and Blaker, A. T.: Ocean and atmosphere influence on the 2015 European heatwave, Environmental Research Letters, 14, https://doi.org/10.1088/1748-9326/ab4d33, 2019.

Meehl, G. A., Moss, R., Taylor, K. E., Eyring, V., Stouffer, R. J., Bony, S., and Stevens, B.: Climate model intercomparisons: Preparing for the next phase, Eos, 95, 77–78, https://doi.org/10.1002/2014EO090001, 2014.

Menary, M. B. and Hermanson, L.: Limits on determining the skill of North Atlantic Ocean decadal predictions, Nature Communications, 9, 1694, https://doi.org/10.1038/s41467-018-04043-9, 2018.

Menary, M. B., Hodson, D. L., Robson, J. I., Sutton, R. T., Wood, R. A., and Hunt, J. A.: Exploring the impact of CMIP5 model biases on the simulation of North Atlantic decadal variability, Geophysical Research Letters, 42, 5926–5934, https://doi.org/10.1002/2015GL064360, 2015.

Mignot, J., García-Serrano, J., Swingedouw, D., Germe, A., Nguyen, S., Ortega, P., Guilyardi, E., and Ray, S.: Decadal prediction skill in the ocean with surface nudging in the IPSL-CM5A-LR climate model, Climate Dynamics, 47, 1225–1246, https://doi.org/10.1007/S00382-015-2898-1/TABLES/2, 2016.

Milinski, S., Maher, N., and Olonscheck, D.: How large does a large ensemble need to be?, Earth System Dynamics, 11, 885–901, https://doi.org/10.5194/esd-11-885-2020, 2020.

Moat, B. I., Sinha, B., Berry, D. I., Drijfhout, S. S., Fraser, N., Hermanson, L., Jones, D. C., Josey, S. A., King, B., Macintosh, C., Megann, A., Oltmanns, M., Sanders, R., and Williams, S.: Ocean Heat Convergence and North Atlantic Multidecadal Heat Content Variability, Journal of Climate, 37, 4723 – 4742, https://doi.org/10.1175/JCLI-D-23-0370.1, 2024.

Müller, W. A., Jungclaus, J. H., Mauritsen, T., Baehr, J., Bittner, M., Budich, R., Bunzel, F., Esch, M., Ghosh, R., Haak, H., Ilyina, T., Kleine, T., Kornblueh, L., Li, H., Modali, K., Notz, D., Pohlmann, H., Roeckner, E., Stemmler, I., Tian, F., and Marotzke, J.: A Higher-resolution Version of the Max Planck Institute Earth System Model (MPI-ESM1.2-HR), Journal of Advances in Modeling Earth Systems, 10, 1383–1413, https://doi.org/10.1029/2017MS001217, 2018.

Nicolì, D., Bellucci, A., Ruggieri, P., Athanasiadis, P., Materia, S., Peano, D., Fedele, G., and Gualdi, S.: The CMCC Decadal Prediction System, Geoscientific Model Development Discussions, pp. 1–28, https://doi.org/10.5194/gmd-2022-181, 2022.

Oldenburg, D., Wills, R. C. J., Armour, K. C., Thompson, L., and Jackson, L. C.: Mechanisms of Low-Frequency Variability in North Atlantic Ocean Heat Transport and AMOC, Journal of Climate, 34, 4733–4755, https://doi.org/10.1175/JCLI-D-20-0614.1, 2021.

Ortega, P., Montoya, M., González-Rouco, F., Mignot, J., and Legutke, S.: Variability of the Atlantic meridional overturning circulation in the last millennium and two IPCC scenarios, Climate Dynamics, 38, 1925–1947, https://doi.org/10.1007/s00382-011-1081-6, 2012.

Ortega, P., Mignot, J., Swingedouw, D., Sévellec, F., and Guilyardi, E.: Reconciling two alternative mechanisms behind bi-decadal variability in the North Atlantic, Progress in Oceanography, 137, 237–249, https://doi.org/10.1016/j.pocean.2015.06.009, 2015.

Ortega, P., Robson, J. I., Menary, M., Sutton, R. T., Blaker, A., Germe, A., Hirschi, J. J., Sinha, B., Hermanson, L., and Yeager, S.: Labrador Sea subsurface density as a precursor of multidecadal variability in the North Atlantic: A multi-model study, Earth System Dynamics, 12, 419–438, https://doi.org/10.5194/esd-12-419-2021, 2021.

Palmer, M. D., Haines, K., Tett, S. F. B., and Ansell, T. J.: Isolating the signal of ocean global warming, Geophysical Research Letters, 34, https://doi.org/10.1029/2007GL031712, 2007.

Palmer, M. D., Roberts, C. D., Balmaseda, M., Chang, Y. S., Chepurin, G., Ferry, N., Fujii, Y., Good, S. A., Guinehut, S., Haines, K., Hernandez, F., Köhl, A., Lee, T., Martin, M. J., Masina, S., Masuda, S., Peterson, K. A., Storto, A., Toyoda, T., Valdivieso, M., Vernieres, G., Wang, O., and Xue, Y.: Ocean heat content variability and change in an ensemble of ocean reanalyses, Climate Dynamics, 49, 909–930, https://doi.org/10.1007/s00382-015-2801-0, 2017.

Passos, L., Langehaug, H. R., Årthun, M., Eldevik, T., Bethke, I., and Kimmritz, M.: Impact of initialization methods on the predictive skill in NorCPM : an Arctic – Atlantic case study, Climate Dynamics, 60, 2061–2080, https://doi.org/10.1007/s00382-022-06437-4, 2023.

Piecuch, C. G., Ponte, R. M., Little, C. M., Buckley, M. W., and Fukumori, I.: Mechanisms underlying recent decadal changes in subpolar North Atlantic Ocean heat content, Journal of Geophysical Research: Oceans, 122, 7181– 7197, https://doi.org/10.1002/2017JC012845, 2017.

Pohlmann, H., Jungclaus, J. H., Köhl, A., Stammer, D., and Marotzke, J.: Initializing decadal climate predictions with the GECCO oceanic synthesis: Effects on the North Atlantic, Journal of Climate, 22, 3926–3938, https://doi.org/10.1175/2009JCLI2535.1, 2009.

Polkova, I., Brune, S., Kadow, C., Romanova, V., Gollan, G., Baehr, J., Glowienka-Hense, R., Greatbatch, R. J., Hense, A., Illing, S., Köhl, A., Kröger, J., Müller, W. A., Pankatz, K., and Stammer, D.: Initialization and Ensemble Generation for Decadal Climate Predictions: A Comparison of Different Methods, Journal of Advances in Modeling Earth Systems, 11, 149–172, https://doi.org/10.1029/2018MS001439, 2019.

Polkova, I., Swingedouw, D., Hermanson, L., Köhl, A., Stammer, D., Smith, D., Kröger, J., Bethke, I., Yang, X., Zhang, L., Nicolì, D., Athanasiadis, P. J., Karami, M. P., Pankatz, K., Pohlmann, H., Wu, B., Bilbao, R., Ortega, P., Yang, S., Sospedra-Alfonso, R., Merryfield, W., Kataoka, T., Tatebe, H., Imada, Y., Ishii, M., and Matear, R. J.: Initialization shock in the ocean circulation reduces skill in decadal predictions of the North Atlantic subpolar gyre, Frontiers in Climate, 5, https://doi.org/10.3389/fclim.2023.1273770, 2023.

Qin, M., Dai, A., and Hua, W.: Quantifying Contributions of Internal Variability and External Forcing to Atlantic Multidecadal Variability Since 1870, Geophysical Research Letters, 47, e2020GL089 504, https://doi.org/10.1029/2020GL089504, e2020GL089504 2020GL089504, 2020.

Rahmstorf, S., Box, J. E., Feulner, G., Mann, M. E., Robinson, A., Rutherford, S., and Schaffernicht, E. J.: Exceptional twentieth-century slowdown in Atlantic Ocean overturning circulation, Nature Climate Change, 5, 475–480, https://doi.org/10.1038/nclimate2554, 2015.

Righi, M., Andela, B., Eyring, V., Lauer, A., Predoi, V., Schlund, M., Vegas-Regidor, J., Bock, L., Brötz, B., De Mora, L., Diblen, F., Dreyer, L., Drost, N., Earnshaw, P., Hassler, B., Koldunov, N., Little, B., Loosveldt Tomas, S., and Zimmermann, K.: Earth System Model Evaluation Tool (ESMValTool) v2.0-technical overview, Geoscientific Model Development, 13, 1179–1199, https://doi.org/10.5194/gmd-13-1179-2020, 2020.

Robson, J., Ortega, P., and Sutton, R.: A reversal of climatic trends in the North Atlantic since 2005, Nature Geoscience, https://doi.org/10.1038/ngeo2727, 2016.

Robson, J., Polo, I., Hodson, D. L., Stevens, D. P., and Shaffrey, L. C.: Decadal prediction of the North Atlantic subpolar gyre in the HiGEM high-resolution climate model, Climate Dynamics, 50, 921–937, https://doi.org/10.1007/S00382-017-3649-2/FIGURES/7, 2018.

Robson, J. I., Sutton, R. T., and Smith, D. M.: Initialized decadal predictions of the rapid warming of the North Atlantic Ocean in the mid 1990s, Geophysical Research Letters, 39, 1–6, https://doi.org/10.1029/2012GL053370, 2012.

Sellar, A. A., Walton, J., Jones, C. G., Wood, R., Abraham, N. L., Andrejczuk, M., Andrews, M. B., Andrews, T., Archibald, A. T., de Mora, L., Dyson, H., Elkington, M., Ellis, R., Florek, P., Good, P., Gohar, L., Haddad, S., Hardiman, S. C., Hogan, E., Iwi, A.,

Jones, C. D., Johnson, B., Kelley, D. I., Kettleborough, J., Knight, J. R., Köhler, M. O., Kuhlbrodt, T., Liddicoat, S., Linova-Pavlova, I., Mizielinski, M. S., Morgenstern, O., Mulcahy, J., Neininger, E., O'Connor, F. M., Petrie, R., Ridley, J., Rioual, J. C., Roberts, M., Robertson, E., Rumbold, S., Seddon, J., Shepherd, H., Shim, S., Stephens, A., Teixiera, J. C., Tang, Y., Williams, J., Wiltshire, A., and Griffiths, P. T.: Implementation of U.K. Earth System Models for CMIP6, Journal of Advances in Modeling Earth Systems, 12, 1–27, https://doi.org/10.1029/2019MS001946, 2020.

Siegert, S., Bellprat, O., Ménégoz, M., Stephenson, D. B., and Doblas-Reyes, F. J.: Detecting improvements in forecast correlation skill: Statistical testing and power analysis, Monthly Weather Review, 145, 437–450, https://doi.org/10.1175/MWR-D-16-0037.1, 2017.

Smith, D. M., Eade, R., and Pohlmann, H.: A comparison of full-field and anomaly initialization for seasonal to decadal climate prediction, Climate Dynamics, 41, 3325–3338, https://doi.org/10.1007/s00382-013-1683-2, 2013.

Smith, D. M., Eade, R., Scaife, A. A., Caron, L.-P., Danabasoglu, G., DelSole, T. M., Delworth, T., Doblas-Reyes, F. J., Dunstone, N. J., Hermanson, L., Kharin, V., Kimoto, M., Merryfield, W. J., Mochizuki, T., Müller, W. A., Pohlmann, H., Yeager, S., and Yang, X.: Robust skill of decadal climate predictions, npj Climate and Atmospheric Science, 2, 1–10, https://doi.org/10.1038/s41612-019-0071-y, 2019.

Smith, D. M., Scaife, A. A., Eade, R., Athanasiadis, P., Bellucci, A., Bethke, I., Bilbao, R., Borchert, L. F., Caron, L. P., Counillon, F., Danabasoglu, G., Delworth, T., Doblas-Reyes, F. J., Dunstone, N. J., Estella-Perez, V., Flavoni, S., Hermanson, L., Keenlyside, N., Kharin, V., Kimoto, M., Merryfield, W. J., Mignot, J., Mochizuki, T., Modali, K., Monerie, P. A., Müller, W. A., Nicolí, D., Ortega, P., Pankatz, K., Pohlmann, H., Robson, J., Ruggieri, P., Sospedra-Alfonso, R., Swingedouw, D., Wang, Y., Wild, S., Yeager, S., Yang, X., and Zhang, L.: North Atlantic climate far more predictable than models imply, Nature, 583, 796–800, https://doi.org/10.1038/s41586-020-2525-0, 2020.

Sospedra-Alfonso, R., Merryfield, W. J., Boer, G. J., Kharin, V. V., Lee, W. S., Seiler, C., and Christian, J. R.: Decadal climate predictions with the Canadian Earth System Model version 5 (CanESM5), Geoscientific Model Development, 14, 6863–6891, https://doi.org/10.5194/gmd-14-6863-2021, 2021.

Sutton, R. T. and Hodson, D. L. R.: Atlantic Ocean Forcing of North American and European Summer Climate, Science, 309, 115–118, https://doi.org/10.1126/science.1109496, 2005.

Swart, N. C., Cole, J. N., Kharin, V. V., Lazare, M., Scinocca, J. F., Gillett, N. P., Anstey, J., Arora, V., Christian, J. R., Hanna, S., Jiao, Y., Lee, W. G., Majaess, F., Saenko, O. A., Seiler, C., Seinen, C., Shao, A., Sigmond, M., Solheim, L., Von Salzen, K., Yang, D., and Winter, B.: The Canadian Earth System Model version 5 (CanESM5.0.3), Geoscientific Model Development, 12, 4823–4873, https://doi.org/10.5194/gmd-12-4823-2019, 2019.

Tietsche, S., Balmaseda, M., Zuo, H., Roberts, C., Mayer, M., and Ferranti, L.: The importance of North Atlantic Ocean transports for seasonal forecasts, Climate Dynamics, 2004, https://doi.org/10.1007/s00382-020-05364-6, 2020.

Titchner, H. A. and Rayner, N. A.: The Met Office Hadley Centre sea ice and sea surface temperature data set, version 2: 1. Sea ice concentrations, Journal of Geophysical Research: Atmospheres, 119, 2864–2889, https://doi.org/10.1002/2013JD020316, 2014.

Volpi, D., Guemas, V., and Doblas-Reyes, F. J.: Comparison of full field and anomaly initialisation for decadal climate prediction: towards an optimal consistency between the ocean and sea-ice anomaly initialisation state, Climate Dynamics, 49, 1181–1195, https://doi.org/10.1007/s00382-016-3373-3, 2017.

Volpi, D., Meccia, V. L., Guemas, V., Ortega, P., Bilbao, R., Doblas-Reyes, F. J., Amaral, A., Echevarria, P., Mahmood, R., and Corti, S.: A Novel Initialization Technique for Decadal Climate Predictions, Frontiers in Climate, 3, 1–14, https://doi.org/10.3389/fclim.2021.681127, 2021.

Yashayaev, I. and Loder, J. W.: Recurrent replenishment of Labrador Sea Water and associated decadal-scale variability, Journal of Geophysical Research: Oceans, 121, 8095–8114, https://doi.org/10.1002/2016JC012046, 2016.

Yeager, S.: The abyssal origins of North Atlantic decadal predictability, Climate Dynamics, 55, 2253–2271, https://doi.org/10.1007/s00382-020-05382-4, 2020.

Yeager, S., Kim, W., and Robson, J.: What caused the Atlantic Cold Blob of 2015?, US CLIVAR Var, 14, 24–31, 2016.

Yeager, S. G., Danabasoglu, G., Rosenbloom, N. A., Strand, W., Bates, S. C., Meehl, G. A., Karspeck, A. R., Lindsay, K., Long, M. C., Teng, H., and Lovenduski, N. S.: Predicting near-term changes in the earth system: A large ensemble of initialized decadal prediction simulations using the community earth system model, Bulletin of the American Meteorological Society, 99, 1867–1886, https://doi.org/10.1175/BAMS-D-17-0098.1, 2018.

Yeager, S. G., Chang, P., Danabasoglu, G., Rosenbloom, N., Zhang, Q., Castruccio, F. S., Gopal, A., Cameron Rencurrel, M., and Simpson, I. R.: Reduced Southern Ocean warming enhances global skill and signal-to-noise in an eddy-resolving decadal prediction system, npj Climate and Atmospheric Science, 6, 107, https://doi.org/10.1038/s41612-023-00434-y, 2023.

Yukimoto, S., Kawai, H., Koshiro, T., Oshima, N., Yoshida, K., Urakawa, S., Tsujino, H., Deushi, M., Tanaka, T., Hosaka, M., Yabu, S., Yoshimura, H., Shindo, E., Mizuta, R., Obata, A., Adachi, Y., and Ishii, M.: The meteorological research institute Earth system model version 2.0, MRI-ESM2.0: Description and basic evaluation of the physical component, Journal of the Meteorological Society of Japan, 97, 931–965, https://doi.org/10.2151/jmsj.2019-051, 2019.

Zanna, L., Khatiwala, S., Gregory, J. M., Ison, J., and Heimbach, P.: Global reconstruction of historical ocean heat storage and transport, Proceedings of the National Academy of Sciences of the United States of America, 116, 1126–1131, https://doi.org/10.1073/pnas.1808838115, 2019.

Zhang, R. and Delworth, T. L.: Impact of Atlantic multidecadal oscillations on India/Sahel rainfall and Atlantic hurricanes, Geophysical Research Letters, 33, https://doi.org/10.1029/2006GL026267, 2006.

Zuo, H., Balmaseda, M. A., Tietsche, S., Mogensen, K., and Mayer, M.: The ECMWF operational ensemble reanalysis-analysis system for ocean and sea ice: A description of the system and assessment, Ocean Science, 15, 779–808, https://doi.org/10.5194/os-15-779-2019, 2019.